ELECTROCHEMICAL PROBING OF CAUSES FOR VARIATION IN LIFETIME OF IRIDIUM-TANTALUN OXIDE ELECTRODE USED IN COPPER ELECTROWINNING

by

Dongni Ma

A Dissertation Submitted to the Faculty of the

DEPARTMENT OF CHEMICAL AND ENVIRONMENTAL ENGINEERING

In Partial Fulfillment of the Requirements

For the Degree of

DOCTOR OF PHILOSOPHY
WITH A MAJOR IN CHEMICAL ENGINEERING

In the Graduate College

THE UNIVERSITY OF ARIZONA

2017

THE UNIVERSITY OF ARIZONA
GRADUATE COLLEGE

As members of the Dissertation Committee, we certify that we have read the dissertation prepared by Dongni Ma, titled Electrochemical Probing of Causes for Variation in Lifetime of Iridium-Tantalum Oxide Electrode Used in Copper Electrowinning and recommend that it be accepted as fulfilling the dissertation requirement for the Degree of Doctor of Philosophy.

_____ Date: (07/06/2017)
Srini Raghavan

_____ Date: (07/06/2017)
Krishna Muralidharan

_____ Date: (07/06/2017)
Eduardo Saez

_____ Date: (07/06/2017)
Paul Blowers

Final approval and acceptance of this dissertation is contingent upon the candidate's submission of the final copies of the dissertation to the Graduate College.

I hereby certify that I have read this dissertation prepared under my direction and recommend that it be accepted as fulfilling the dissertation requirement.

_____ Date: (07/06/2017)
Dissertation Director: Srini Raghavan

STATEMENT BY AUTHOR

This dissertation has been submitted in partial fulfillment of the requirements for an advanced degree at the University of Arizona and is deposited in the University Library to be made available to borrowers under rules of the Library.

Brief quotations from this dissertation are allowable without special permission, provided that an accurate acknowledgement of the source is made. Requests for permission for extended quotation from or reproduction of this manuscript in whole or in part may be granted by the head of the major department or the Dean of the Graduate College when in his or her judgment the proposed use of the material is in the interests of scholarship. In all other instances, however, permission must be obtained from the author.

SIGNED: Dongni Ma

ACKNOWLEDGEMENTS

First, I would like to express my deepest appreciation and gratitude to my advisor—Dr. Srini Raghavan—for his patient guidance and wise mentorship, beginning in 2013 when I joined his research group and continuing through the completion of my doctorate in chemical engineering. He not only taught me how to conduct research but also how to behave in life.

I would also like to thank my committee members: Dr. Eduardo Saez, for all his help during my graduate studies, and Dr. Paul Blowers, for his support and for serving as one of my committee members. I thank Dr. Krishna Muralidharan for his help and guidance in the study of my minor subject.

I am grateful to all my current and past research colleagues for their assistance with my studies: Bing Wu, Clovis Weisbart, Ryan O'Connell, Vanda Ngo, Yusuke Watanabe, Mingrui Zhao, Tony Gnanaprakasa, Selene Sandoval, Chieh-Chun Chiang, Rajesh Balachandran, and Xiaoyang Ji.

I thankfully acknowledge Freeport-McMoRan Inc. for providing the financial support and Scot Sandoval of Freeport McMoran Technical Center for all his assistance on my project.

Last but not least, I would like to thank my parents (Qingping Tian and Yuxin Ma) for their support and faith in me as I pursued my degree.

DEDICATION

I would like to dedicate this dissertation to my parents Qingping Tian and Yuxin Ma.

TABLE OF CONTENTS

TABLE OF CONTENTS-*Continued*

TABLE OF CONTENTS-*Continued*

LIST OF FIGURES

LIST OF FIGURES-*Continued*

LIST OF FIGURES-*Continued*

LIST OF FIGURES-*Continued*

LIST OF FIGURES-*Continued*

LIST OF FIGURES-*Continued*

LIST OF TABLES

LIST OF TABLES-*Continued*

ABSTRACT

In hydrometallurgical copper production plants, titanium-based electrodes coated with a conductive layer of IrO_2-Ta_2O_5 are widely used as anodes in acidic copper electrowinning baths because of their long service life and low overpotential for oxygen evolution. The presence of trace amounts of ions such as fluoride, aluminum, and iron in sulfate-based electrowinning baths is believed to affect the stability of IrO_2-Ta_2O_5 coated anodes. Hence, in this study, the effect of fluoride and metallic cations on the lifetime of IrO_2-Ta_2O_5 coated Ti electrodes in sulfuric acid solutions has been investigated, and a degradation mechanism for IrO_2-Ta_2O_5 coatings in the presence of fluoride has been proposed.

Typical lifetime of the conductive ceramic coated anodes is 1 to 2 years. In order to predict electrode performance over this long period, an accelerated laboratory test that can be carried out in a few weeks is often used. This test, known as accelerated lifetime test (ALT), is conducted by electrically stressing the anodes at a current density that is much higher than the current density used for electrowinning while monitoring the change in the cell potential. The time required for the cell voltage to increase by 5 V is taken as the accelerated lifetime of the oxide electrode. In this research, titanium mesh samples coated with mixed iridium oxide-tantalum oxide layers were tested as anodes in 2 M sulfuric solution a constant current density of 0.54 A/cm^2. A two-electrode cell with a bare titanium mesh serving as the cathode was used for experiments.

In addition to ALTs, anodic polarization measurements were also carried out to study the changes in overpotential for oxygen evolution on electrodes before and after ALTs. Additionally, morphology and chemical composition analyses were performed on electrodes before and after ALTs using various techniques such as scanning electron microscopy (SEM) analysis, energy-

dispersive X-ray spectroscopy (EDS), X-ray diffraction (XRD), and X-ray photoelectron spectroscopy (XPS). Chemical species that are likely to be present in the electrowinning bath were predicted using the computer software STABCAL and presented in distribution-pH and Pourbaix diagrams.

The results of multiple ALTs in the absence and presence of various levels of fluoride indicate that the anode lifetime was greatly reduced by the presence of fluoride in sulfuric acid solutions. The greater the amount of fluoride added, the shorter the anode lifetime. Additionally, both in the absence and presence of fluoride, the molar ratio of IrO_2 to Ta_2O_5 in the coating did not change during dissolution. In studying strategies to prolong the lifetime of the electrode in a fluoride-containing solution, a method of complexing fluoride ions using metallic cations such as Al^{3+} and Fe^{3+} was developed and demonstrated. The anode lifetime was successfully prolonged from 200 to over 500 hours with the addition of aluminum ions to a fluoride-containing solution. Compared with ferric ions, aluminum ions are more efficient in complexing with fluoride to extend the lifetime of electrodes.

CHAPTER 1

INTRODUCTION

1.1 Introduction to copper electrowinning

Copper is used in a wide variety of applications in modern life. It occurs in nature in the form of native copper and in copper sulfide, oxide, silicate, and carbonate compounds commonly referred to as copper ores. To extract copper from ore, either a pyrometallurgical or hydrometallurgical process can be used. These processes are shown schematically in Figure 1.

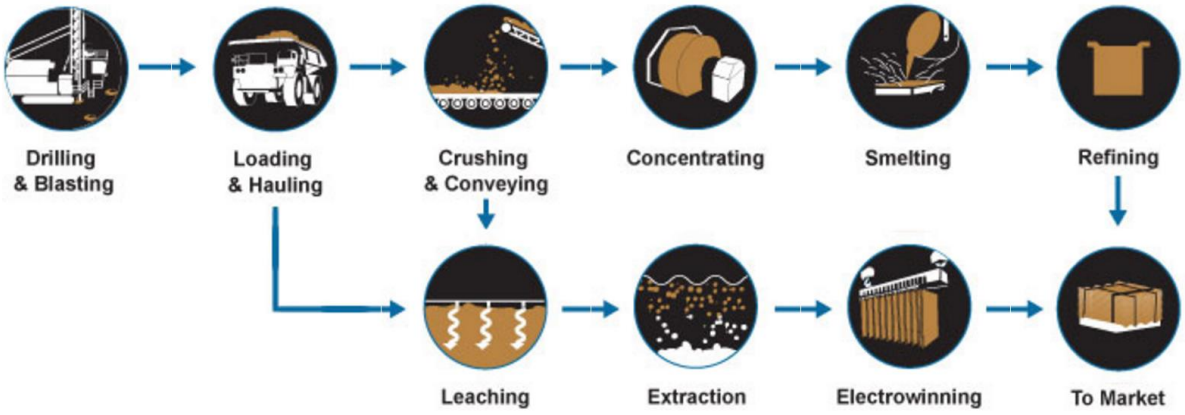

Figure 1. Steps involved in copper production (Courtesy: Freeport-McMoRan Inc [1].)

The hydrometallurgical process used to extract copper from ores involves several steps, which include the processing of mined ore by crushing and grinding, leaching (extraction) with sulfuric acid, solvent extraction (SX) to selectively transfer copper ions to an organic phase, stripping with sulfuric acid to transfer the copper ions back to the aqueous phase at a higher concentration, and electrowinning (EW) to produce high-purity copper.

The key steps in the hydrometallurgical process are solvent extraction and electrowinning. The solvent extraction process consists of two steps, extraction and stripping. In the extraction step, the aqueous solution from the leaching process, which contains a few grams per liter of copper ions, is placed in contact with an inert organic solvent containing a chemical (aka extractant) that selectively chelates or complexes copper ions. Copper is extracted away from the aqueous phase into the organic phase, leaving behind impurities. In the stripping step, the organic phase containing the copper is stripped of copper through contact with a strongly acidic aqueous solution. At the end of the stripping step, the copper ion concentration in the stripping solution is increased to an order of magnitude larger than that of the leach solution. Finally, in the electrowinning process, copper ions in the acidic solution are electrochemically reduced to copper layers on a cathode. In a typical electrowinning plant, in a period of six to seven days, approximately 100-300 pounds of copper with a purity of 99.99% is deposited onto the cathodes.

A schematic of a typical copper electrowinning cell is shown in Figure 2.

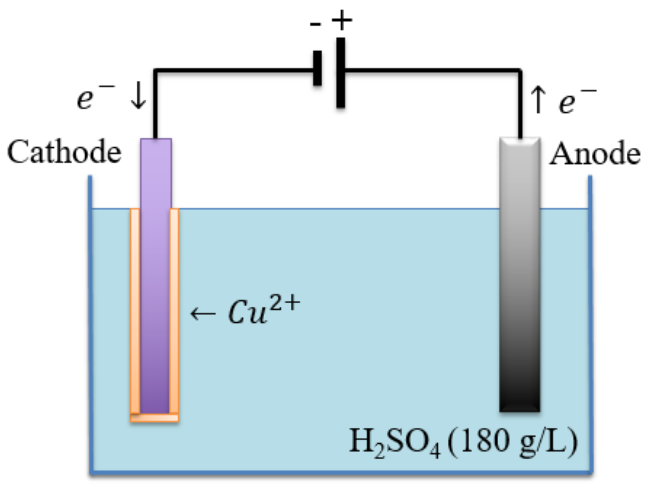

Figure 2. A schematic of a typical copper electrowinning cell.

The cell consists of an anode (positive electrode), a cathode (negative electrode), and an electrolyte, which is typically made up of 180 g/L sulfuric acid and 30–40 g/L Cu^{2+} ions. When a current or potential is applied to the cell, water decomposes to form oxygen, and electrons are produced at the anode. The copper ions migrate to the cathode where they are reduced to form solid copper at the cathode. The reactions that take place at the anode and the cathode are shown below:

$$\text{Anode: } 2H_2O \rightarrow O_2 \uparrow +4H^+ + 4e^- \quad E^0 = 1.23\,V$$

$$\text{Cathode: } Cu^{2+} + 2e^- \rightarrow Cu \quad E^0 = 0.34\,V$$

Commonly, the materials used for the anode are lead based (lead with 6% antimony, lead with 0.7% calcium and 1.3% tin, and lead with 0.05% strontium and 0.6% tin) [2] or involve a Ti substrate coated with IrO_2-Ta_2O_5. The cathode is typically a stainless steel plate. Current density and potential values commonly used in copper electrowinning are 0.18 A/cm^2 and 2.5 V, respectively.

In addition to the desired copper ions, the electrowinning baths from various industrial locations contain fluoride (10–160 ppm), aluminum (400–2000 ppm), iron (2000–3000 ppm), and other ions such as calcium and manganese. The possible concentration ranges for these other compounds are broad due to the variability in the composition of the processed ores.

1.2 Explanation of the problem and research objectives

Titanium-based dimensionally stable anodes (DSAs®) coated with an electrocatalytically active layer of IrO_2-Ta_2O_5 formed by thermal decomposition are commonly used in sulfate-based copper electrowinning plants. These anodes are used because of their high durability and low overpotential for oxygen evolution [2], but they are quite expensive. The lifetime of these electrodes is typically a few years but is known to vary depending on the geographical location of the metallurgical plant. One of the culprits for this variability is postulated to be the presence of fluoride in the electrowinning baths. Fluoride ions can form HF in an acidic environment and can damage the IrO_2-Ta_2O_5 active layer.

The objective of this project is to investigate the effect of fluoride ions in sulfuric acid solutions on the stability and lifetime of the IrO_2-Ta_2O_5–coated Ti mesh electrodes through both electrochemical studies and morphological analysis. The ultimate objective is to develop methodologies such as complexation with metal cations to prolong the lifetime of the electrode in fluoride-containing solutions.

CHAPTER 2

BACKGROUND AND LITERATURE REVIEW

2.1 Background theory

2.1.1 Butler-Volmer relationship and Tafel slope

The amount of current I (A) or current density i (A/cm^2) generated from an electrochemical reaction as a function of potential can be expressed using the Butler-Volmer relationship in Equations (2.1) and (2.2) [3-6]:

$$i = i_a - i_c = \text{anodic current density} - \text{cathodic current density} \quad (2.1)$$

$$i = i_0 \left\{ exp\left[\frac{\alpha n F \eta}{RT}\right] - exp\left[-\frac{(1-\alpha) n F \eta}{RT}\right]\right\} \quad (2.2)$$

where i = net current density, i_0 = exchange current density, which is the measure of the rate of oxidation and reduction at equilibrium, η = overpotential (applied potential E – equilibrium potential E_{eq}), α = anodic transfer coefficient, F = Faraday constant, 96500 C/mol, n = number of electrons involved in the electrochemical reaction, R = gas constant, 8.314 J/(mol K), and T = absolute temperature, K.

Assuming i_0 = 10^{-5} A/cm^2, α = 0.5, n = 1, and T = 298 K, an example of a Butler-Volmer plot is provided in Figure 3. From the data in this figure, taking the absolute value of the measured current density (i) and plotting it in a Tafel plot, which is a figure of overpotential (η) as a function of the measured current density (i) (in Figure 4 [7]).

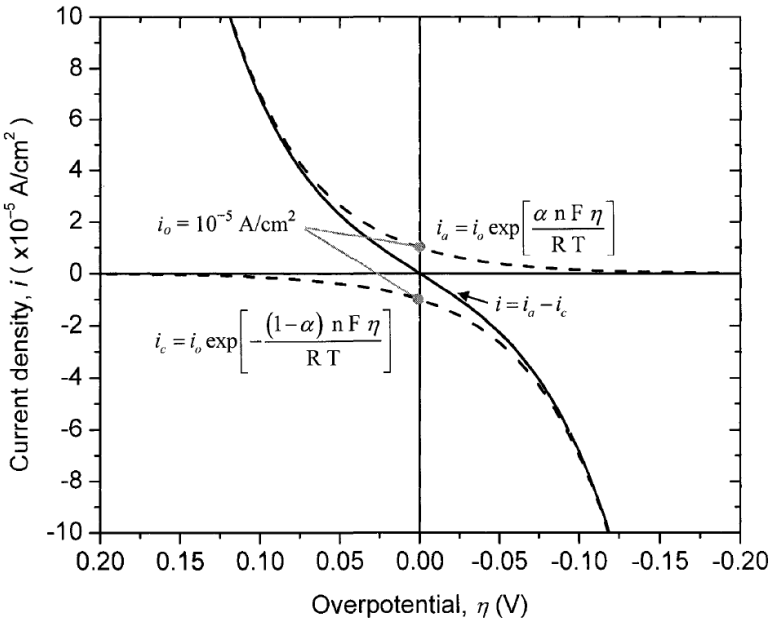

Figure 3. Example of the Butler-Volmer equation assuming i_0 = 10^{-5} A/cm^2, α = 0.5, n = 1, and T = 298 K [7].

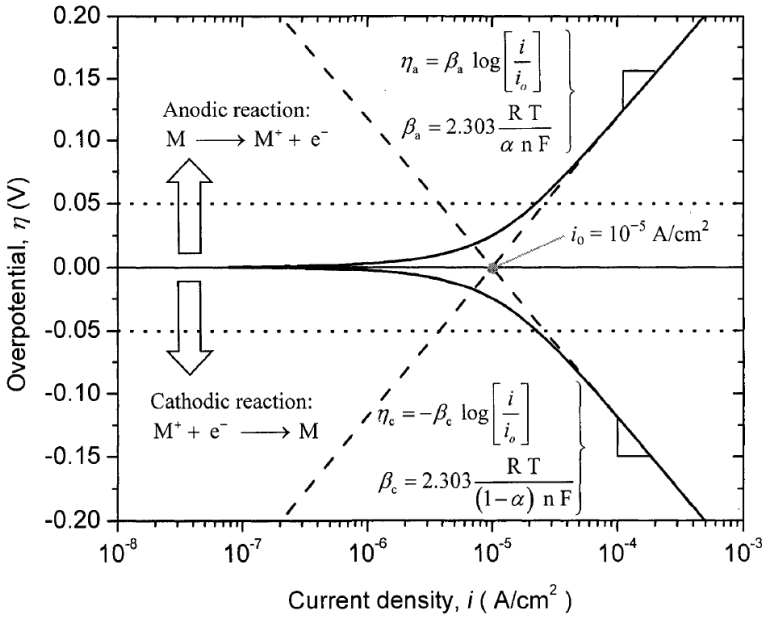

Figure 4. Tafel relationship (semi-log plot) derived from Figure 3 at an overpotential (η) larger than ± 0.05 V [7].

A linear relationship is formed between η and log (i) when the overpotential η is larger than ± 0.05 V. This relationship is known as the Tafel relationship as described in Equations (2.3) and (2.4) [8].

Anodic: $\eta_a = \beta_a \, log\left[\frac{i}{i_0}\right]$, where $\beta_a = 2.303 \, \frac{R\,T}{\alpha n F}$ (2.3)

Cathodic: $\eta_b = -\beta_c \, log\left[\frac{i}{i_0}\right]$, where $\beta_c = 2.303 \, \frac{R\,T}{(1-\alpha) n F}$ (2.4)

Because of the assumption that the transfer coefficient α = 0.5, the anodic and cathodic current densities in Figure 4 are symmetric.

The oxygen evolution reaction takes place on the anode, so only the anodic section will be taken into consideration in this dissertation. An example of an anodic polarization measurement result is shown in Figure 5 by Yang and his coworkers [9]. They studied the electrocatalytic performances on several electrodes such as IrO_2-Ta_2O_5 coated Ti, Pb-Ag, and Pb electrodes. The polarization measurements were carried in 0.5 M H_2SO_4 solutions.

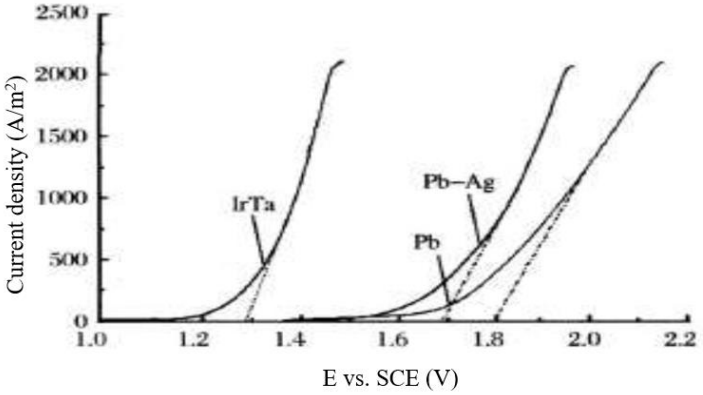

Figure 5. Steady-state polarization curve of the anodic oxygen evolution reaction (1 mV/s, 25°C) [9].

To calculate oxygen overpotential, a tangent line is drawn to the curves in the region where the current density starts increasing rapidly. The intersection of the tangential line with the x-axis is the onset measured potential E_m used to calculate the overpotential using Equations (2.5) and (2.6) [10].

$$E_1 = E_m - iR \tag{2.5}$$

$$\eta_{O_2} = E_1 + E_2 - E_{O_2/H_2O} \tag{2.6}$$

In the above equations, η_{O_2} is the overpotential for oxygen evolution, E_1 represents the measured potential between the anode and the reference electrode after elimination of the iR ohmic drop (i is the measured current density, and R is the resistance of the electrolyte used), E_2 is the potential for the reference electrode at 25°C, and E_{O_2/H_2O} is the reduction potential of oxygen to water at 25°C and at the pH of the solution [10].

2.1.2 Pourbaix diagrams

In order to predict which chemical species form is stable in acidic solutions with applied potential, a potential-pH, or Pourbaix diagram becomes common practice. It is constructed to provide a fundamental understanding of the thermodynamically favorable species in the investigated system. It can be considered as a two-dimensional phase diagram with pH and potential as master variables. The construction requires Gibbs free energy data for species that can exist in the chemical system under consideration. In this work, Pourbaix diagrams were constructed using the computer software STABCAL.

2.2 Why IrO_2-Ta_2O_5 coated Ti electrodes?

In copper electrowinning baths, the basic standards used to select anodes in sulfate-based solutions are electrochemical stability, resistance to chemical corrosion in a strong acidic environment, low overpotential for oxygen evolution, mechanical stability, and environmental safety [2]. Lead-based electrodes have been used as traditional anodes in copper electrowinning because of their low cost of fabrication. They typically contain Pb, Sb, and Ca and minor amounts of other elements. However, lead-based electrodes have some drawbacks, such as their low corrosion resistance, their poor stability, and the harm they might cause to the environment. Therefore, researchers have explored alternative materials and found a replacement for lead-based electrodes called dimensionally stable anodes (DSAs®). Compared with lead-based electrodes, DSAs® exhibit both high corrosion resistance and electrochemical activity for oxygen evolution [2]. These anodes commonly consist of mixed metal oxide coatings on titanium or zirconium substrates. The oxides used to form coatings include tantalum oxide (Ta_2O_5), iridium oxide (IrO_2), ruthenium dioxide (RuO_2), and tin oxide (SnO_2) [11–14]. Among them, IrO_2 (70 mol%)-Ta_2O_5 (30 mol%) coated electrodes have been reported to be the best for oxygen evolution in acidic solutions because of their high electrocatalytic activity and stability (service lifetime can be approximately 2-3 years at a current density of 0.18 A/cm^2). Binary coatings with IrO_2, RuO_2, and Pt as active components with TiO_2, ZrO_2, and Ta_2O_5 as inert matrix material on Ti substrates have also been explored [11]. Additional details on investigations into IrO_2-Ta_2O_5 coated Ti substrate electrodes will be presented in sections 2.3 to 2.5.

The most common method used to prepare the IrO_2-Ta_2O_5 coating is thermal decomposition. In this method, iridium and tantalum chloride precursors are first dissolved in an

alcoholic or aqueous solution and then brush-coated in multiple layers on Ti substrates. This is followed by heat treatment around 400 °C to achieve desired coating thickness [15].

2.3 Studies on the electrochemical activity of IrO_2-Ta_2O_5 coated Ti electrodes

Many investigations into the electrochemical properties of IrO_2-Ta_2O_5 binary oxide electrodes in basic or acidic solutions have been reported [2, 16-20]. A laboratory technique known as the accelerated lifetime test (ALT) is commonly used to predict the lifetime of the electrodes within a much shorter time period than their industrial service life. This measurement uses a galvanostatic method that applies a constant current density to the electrode while the changes in cell potential are monitored as a function of time. After a period of experiment, the IrO_2-Ta_2O_5 coating is detached from Ti substrate leading the formation of TiO_2 passivation layer and a rise in cell potential. Hence, the accelerated lifetime is defined as the time at which a significant rise (5–10 V) is observed in the cell potential from the constant potential value attained after the current is applied.

2.3.1 Variations in chemical composition of IrO_2-Ta_2O_5 coated Ti electrodes

The electrochemical properties of IrO_2-Ta_2O_5 coated Ti electrodes with various nominal amounts of IrO_2 have been investigated by many researchers in acidic/neutral/alkaline solutions. Results indicate that the electrode with 70 mol% IrO_2 has the best electrocatalytic and stability regardless of selected electrolytes. For instance, the electrocatalytic properties of electrodes with various nominal amounts of IrO_2 (10, 40, 70, and 100 in mol%) have been reported by Li and coworkers [21] using potentiodynamic polarization and other techniques. Potentiodynamic polarization measurements were performed at a scan rate of 10 mV/s on prepared electrodes in 0.5 M H_2SO_4 solution at 25°C using a three-electrode system (with a platinum foil used as the counter

electrode and a saturated calomel electrode (SCE) as the reference electrode). The current measured at the oxygen evolution potential (1.5 V vs SCE) for various nominal contents of IrO_2 are shown in Figure 6.

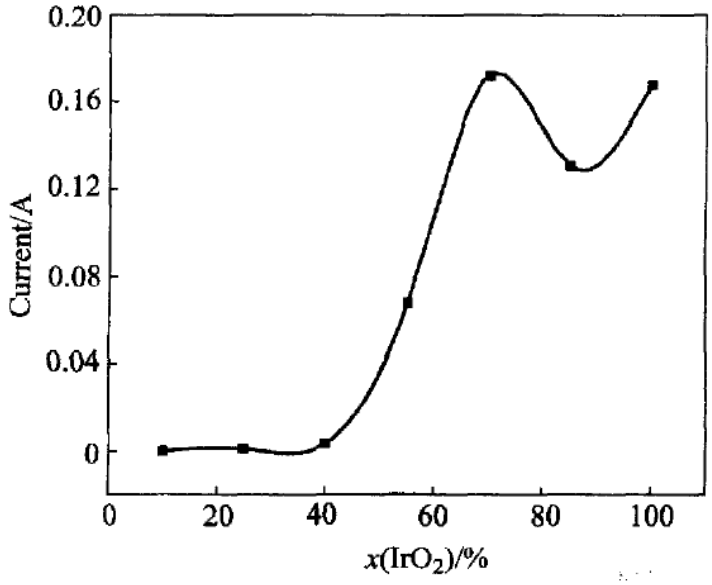

Figure 6. Current for E = 1.5 V (vs. SCE) on Ti/IrO_2-Ta_2O_5 anodes with various amounts of IrO_2 (x indicates mol%) [21].

As depicted in Figure 6, the current at a given potential of 1.5 V (vs. SCE) on IrO_2-Ta_2O_5 coated Ti electrodes increases as the IrO_2 content increases from 40% to 70%. At 70% IrO_2, the current reaches its maximum value, suggesting that IrO_2-Ta_2O_5 electrodes with 70 mol% IrO_2 have the highest electrocatalytic activity for the oxygen evolution reaction.

The electrochemical properties of IrO_2-Ta_2O_5 (10–90 mol% Ir) coated Ti anodes were investigated by Xu and his coworkers [19, 20] in 0.5 M Na_2SO_4 solutions using potentiodynamic polarization measurements and other methods. Figure 7 shows the effect of the oxide composition in the IrO_2-Ta_2O_5 coating on the current density for oxygen evolution.

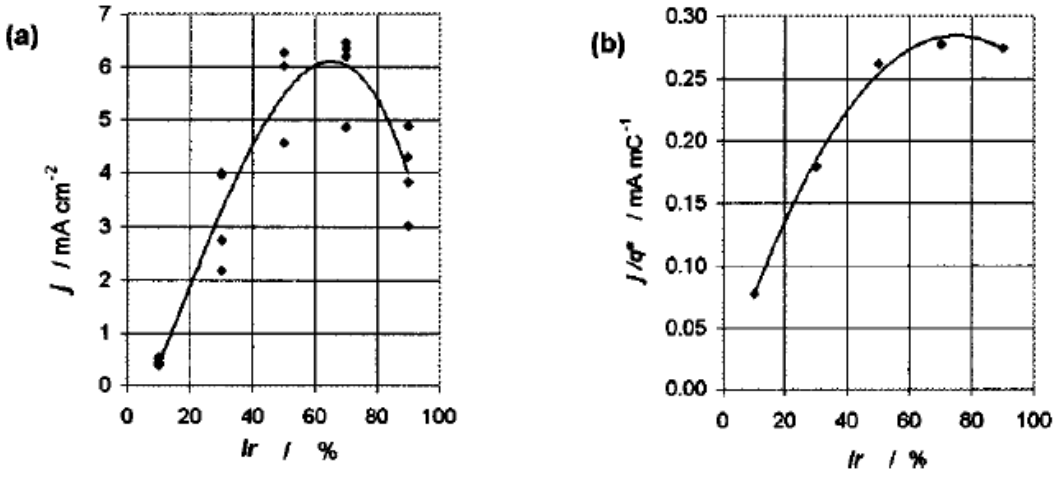

Figure 7. Change of (a) current density and (b) current divided by voltammetric charge of oxygen evolution in 0.5 M Na_2SO_4 with Ir content (j is current density and q* is voltammetric charge) [19].

As shown in Figure 7a, the current density increases as the Ir content increases from 10 to 60%, reaching a maximum value at approximately 70% Ir. Figure 7b shows the current divided by the voltammetric charge. The voltammetric charge was calculated by integrating the regions between the hydrogen and oxygen evolution region in a cyclic voltammetry curve, which has been proven to be proportional to the electrochemical active surface area [22]. Hence, the curve in Figure 7b is related to the real electrocatalytic activity and it increases as the Ir content increases, which is similar to the trend shown in Figure 7a. Based on the results presented in the two figures, it may be concluded that the electrocatalytic activity of IrO_2-Ta_2O_5 coated Ti electrodes can be enhanced by increasing the amount of Ir in the oxide coating. ALTs were also conducted on IrO_2-Ta_2O_5 (10–90 mol% Ir) coated Ti anodes at a current density of 2 A/cm^2 in 1 M H_2SO_4, as shown in Figure 8.

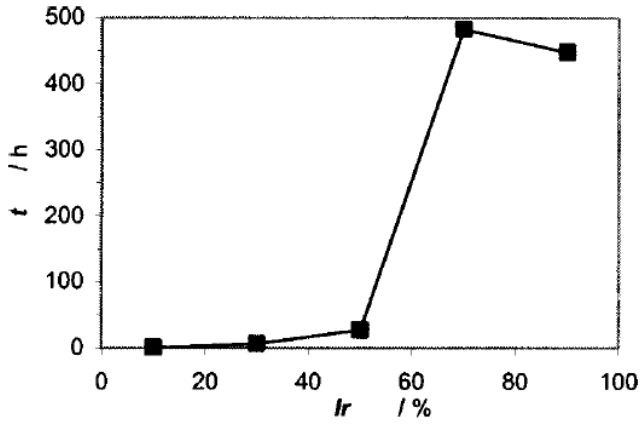

Figure 8. The accelerated lifetime of IrO_2-Ta_2O_5 anodes in 1 M H_2SO_4 at a current density of 2 A/cm^2 [23].

As shown in Figure 8, the accelerated lifetime of the electrode is longest (~500 hours) for the electrode containing 70 mol% IrO_2, while the lifetime is shorter (~450 hours) for 90% mol IrO_2 and significantly shorter on electrodes containing 10, 30, and 50 mol% IrO_2. Therefore, the stability of the electrode is affected by the ratio of IrO_2 to Ta_2O_5 in the oxide coating.

The lifetime of the IrO_2-Ta_2O_5 (70:30 mol%) films in alkaline solutions was studied by Morimitsu and his coworkers [24] as a function of the thickness (weight) of the films. A constant current density of 1 A/cm^2 was applied to the electrodes in a 4 M NaOH solution, and the results of changes in the cell potential as a function of time are provided in Figure 9a. From the data in Figure 9a, it is clear that the accelerated lifetime is dependent on the thickness of the coating.

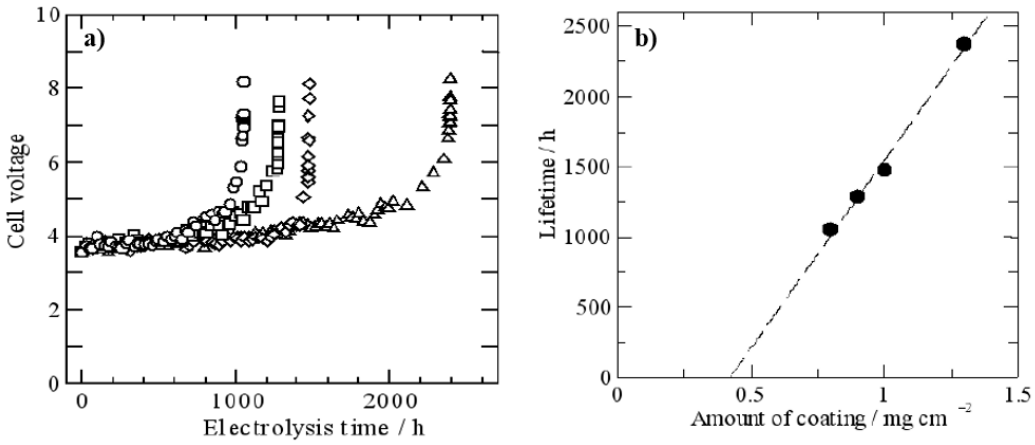

Figure 9. a) Variations in cell voltage during the electrolysis of IrO_2-Ta_2O_5 (70:30 mol%)/Ti electrodes at 1 A cm^{-2} in a 4 M NaOH solution at 323 K. Amount of oxide coating: 0.8 mg cm^{-2} (°), 0.9 mg cm^{-2}(□), 1.0 mg cm^{-2}(◊), and 1.3 mg cm^{-2} (Δ). b) Dependence of the electrode's lifetime on the amount of IrO_2-Ta_2O_5 (70:30 mol%) coating for electrolysis at 1 A cm^{-2} in a 4 M NaOH solution at 323 K [24].

In fact, Figure 9b shows that the lifetime of the electrodes exhibits a linear relationship with the weight of the oxide coating. The slope (2665 h cm^2 mg^{-1}) represents the electrolysis time per unit amount of oxide coating and is very close to that of the electrode in sulfuric acid solutions. Hence, the results indicate that the durability of the electrode in an alkaline solution is comparable to the durability in acidic solutions.

2.3.2 Different preparation methods for IrO_2-Ta_2O_5 coated Ti electrodes

Thermal decomposition is the most common method used to prepare IrO_2-Ta_2O_5–coated Ti electrodes. In this method, iridium and tantalum chloride precursors are dissolved in an alcoholic or aqueous solution and then brush-coated in multiple layers on Ti substrates to form oxide coatings [15]. Researchers found that the microstructure and electrochemical performance

of the electrode are affected by the preparation method [25,26]. The traditional thermal decomposition method is inexpensive but suffers from compositional segregation or precipitates in the microstructure, which influences the electrochemical properties of the electrode [18].

The effects of the oxide coating preparation methods on the electrochemical properties of the electrodes were studied by Xu *et al*. [18]. They prepared the electrodes using a sol-gel method in which two precursors H_2IrCl_6 and $TaCl_5$ were dissolved in a mixed solution of citric acid and ethylene glycol at 60°C and then brush-coated in several layers onto Ti substrates. The coating was dried at 120°C for 10 min, then fired at 500°C for 10 min. A comparison of the morphological features of IrO_2-Ta_2O_5 (70:30 mol%) electrodes prepared by the sol-gel (aka Pechini) method and the traditional method are provided in Figure 10 in the form of scanning electron microscope (SEM) micrographs [10]. On the electrodes prepared by the traditional thermal decomposition method (A), many crystalline precipitates are either scattered in the flat areas or along the ridges. On the surface of the electrodes prepared by the Pechini method, very few particulates and agglomerates are present, and the surface appears more uniform.

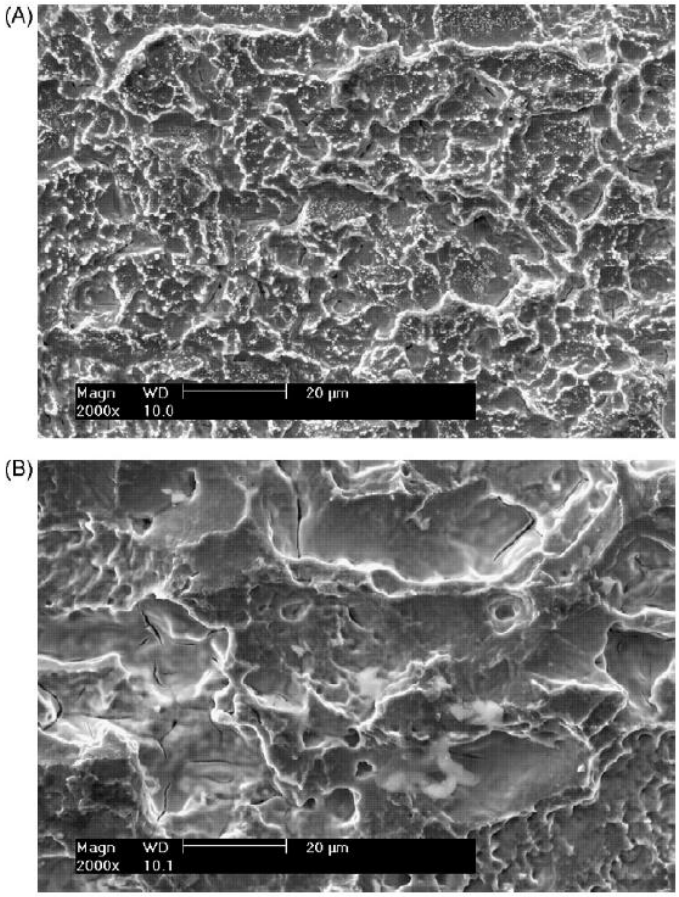

Figure 10. SEM micrographs (magnification of 2000×) of the Ti/IrO_2–Ta_2O_5 electrodes prepared by the conventional thermal decomposition route (a) and the Pechini method (b) [18].

Results from potentiodynamic polarization experiments carried out on electrodes prepared via the sol-gel method are shown in Figure 11.

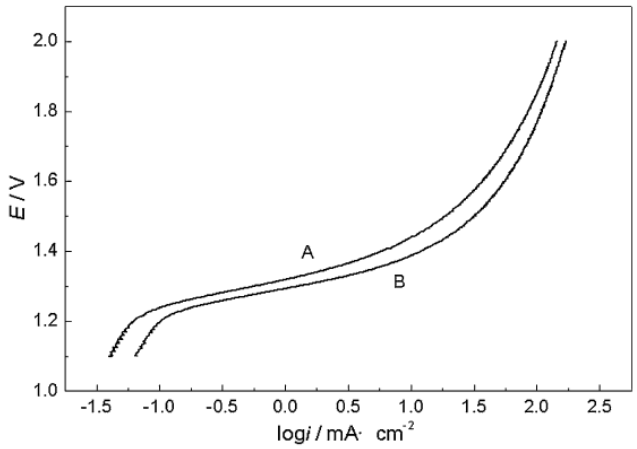

Figure 11. Anodic polarization curves for the Ti/IrO_2–Ta_2O_5 electrodes prepared by the conventional thermal decomposition route (a) and the Pechini method (b) obtained in a 1 M H_2SO_4 solution at a sweep rate of 0.5 mVs^{-1} [18].

From the polarization curves, it is evident that the electrode prepared by the conventional method is characterized by a smaller current density (at a given potential) than the one prepared by the Pechini method, suggesting that the oxide electrodes prepared by the sol-gel method perform better electrochemically in terms of oxygen evolution. Additionally, ALTs were performed on electrodes at a current density of 2 A/cm^2 in 1 M H_2SO_4 solutions. The one prepared by the Pechini method exhibited a longer lifetime (750 hours) than the ones prepared by the conventional method (500 hours). The deactivation of the electrode in ALTs is due to the penetration of the electrolyte to the substrate, causing the formation of a passivation layer between the coating and substrate. Therefore, the more uniform surface prepared by the sol-gel method provides fewer opportunities for the electrolyte to go through the oxide coating and thus prolongs the lifetime of the electrode.

The effects of lowering the coating formation temperature on the morphology and electrochemical activity were investigated by Morimitsu *et al*. [27]. They prepared IrO_2-Ta_2O_5 (80 and 50 mol% Ir) coated electrodes using thermal decomposition temperatures below 400°C. Lowering the temperature resulted in the formation of amorphous IrO_2, which altered the electrochemical activity of the electrode. A comparison of the morphology of the coatings with 80 mol% Ir prepared at 470°C (A) with coatings of 50 mol% Ir prepared at 380°C (B) are shown in Figures 12 and 13.

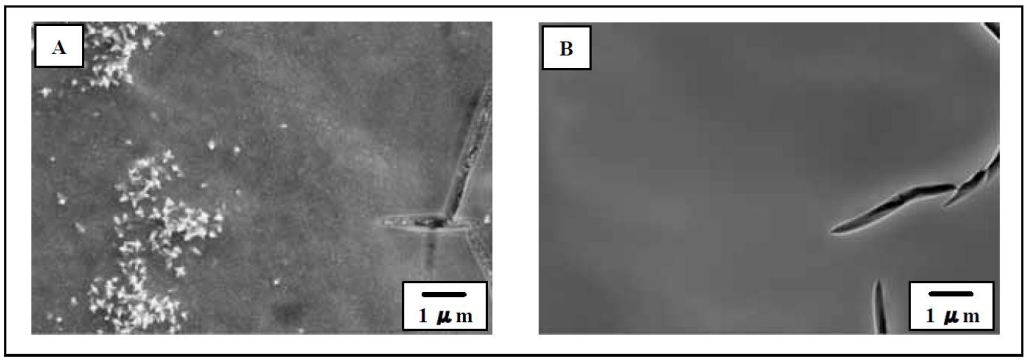

Figure 12. Surface morphologies of the coatings with 80 mol% Ir prepared at 470°C (A) and with 50 mol% Ir prepared at 380°C (B). Magnification: 10,000× [27].

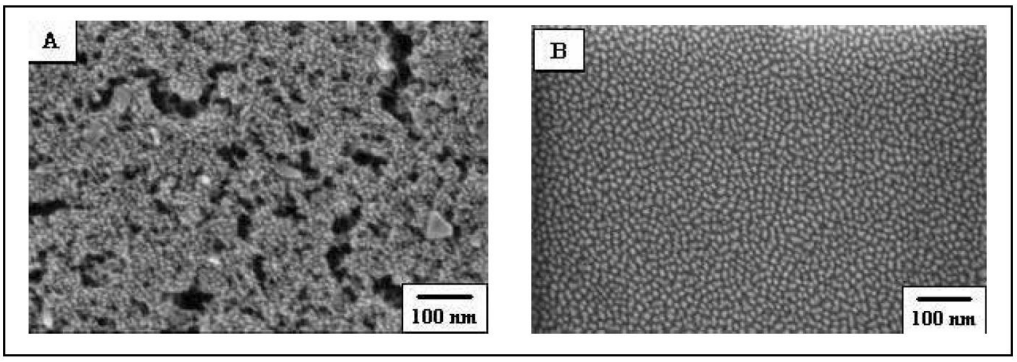

Figure 13. Surface morphologies of the coatings with 80 mol% Ir prepared at 470°C (a) and with 50 mol% Ir prepared at 380°C (b). Magnification: 130,000× [27].

From the low-magnification (10,000×) SEM micrographs of electrodes prepared at two different temperatures shown in Figure 12, it is evident that the surface of the electrode prepared at 470°C exhibits cracks, agglomerates, and flat areas. The surface of the electrode prepared at 380°C is flat and smooth, with some cracks. In the high-magnification SEM micrograph shown in Figure 13a (obtained using a low 1 keV accelerating voltage for the electron beam), the surface of the electrode prepared at the higher temperature actually consists of nanoholes and cracks. This porous surface is also covered with 20–60 nm IrO_2 particles. For the electrode prepared at the lower temperature that is shown in Figure 13b, the surface is made of highly ordered nano IrO_2 particles (5–10 nm in size) surrounded by a Ta_2O_5 matrix.

The lifetime of this amorphous IrO_2-Ta_2O_5/Ti electrode prepared at 380°C was evaluated in another of the author's publications [28]. The lifetime was 4100 hours in a sulfuric acid solution at an applied current density of 1 A/cm^2 at 50°C. This result was close to the lifetime of the normal crystalline IrO_2-Ta_2O_5/Ti electrode, suggesting the durability of the electrode prepared at the lower temperature.

2.3.3 Oxygen evolution studies on IrO_2-Ta_2O_5 coated Ti electrodes

The advantages of using IrO_2-Ta_2O_5 coated Ti electrodes as anodes are that they are highly stable and they exhibit a low overpotential for oxygen evolution, suggesting a possible reduction in energy consumption. Hu *et al.* [29] investigated the oxygen evolution reaction on IrO_2-Ta_2O_5 coated Ti electrodes in a sulfuric acid solution using anodic polarization measurements. Their results are presented in Figure 14.

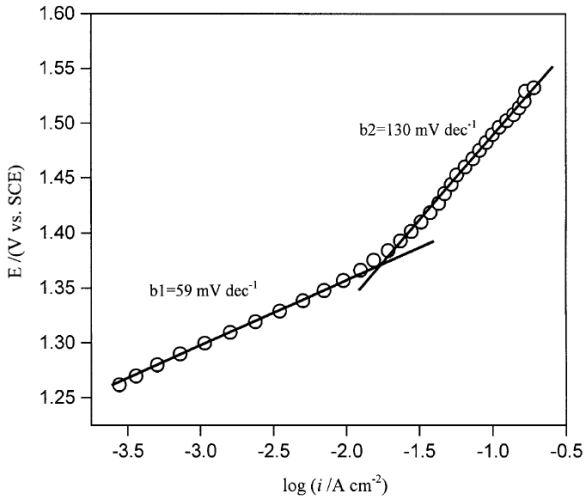

Figure 14. Steady-state polarization curve for the Ti/IrO_2–Ta_2O_5 anode in a H_2SO_4 solution at 25°C (dec represents decades in current changes) [29].

In this figure, the potential E is the effective potential after iR compensation of the applied potential, E_{appl}, as shown in the equation below:

$$E = E_{appl} - iR \tag{2.1}$$

The polarization curve indicates two Tafel slopes, one (59 mV/dec) in the low current density region and the other (130 mV/dec) in the high current density region. The values of the two slopes are close to the ones reported for IrO_2–based electrodes [30]. Da Silva *et al.* [31] proposed a mechanism for the oxygen evolution reaction consisting of the following steps:

$$S + H_2O \rightarrow S - OH_{ads} + H^+ + e^- \tag{R1}$$

$$S - OH_{ads} \rightarrow S - O_{ads} + H^+ + e^- \tag{R2}$$

$$S - O_{ads} \rightarrow S + (\frac{1}{2})O_2 \quad \text{(R3)}$$

In the above steps, S represents the active sites on the electrode surface, and S-OH_{ads} and S-O_{ads} are the adsorbed intermediates formed during the overall reaction. Based on the above mechanism, if step R1 is the rate-determining step, the Tafel slope would be 120 mV/dec. If step 2 or 3 is rate controlling, the slope would be 40 mV/dec or 30 mV/dec, respectively [30].

However, the above mechanism could not explain the slopes provided in Figure 14. Therefore, Hu and his coworkers modified the steps as follows:

$$S + H_2O \rightarrow S - OH^*_{ads} + H^+ + e^- \quad \text{(R1′)}$$

$$S - OH^*_{ads} \rightarrow S - OH_{ads} \quad \text{(R1″)}$$

where $S - OH^*_{ads}$ and $S - OH_{ads}$ are intermediates with the same chemical structures but different energy states. The reactions R1′ and R1″ are rate-determining steps, and the other reactions R2 and R3 occur more quickly. They then mathematically deduced the values of the Tafel slopes and found that the concentration of H^+ in the electrolyte affected the value of the slopes; this explains why they obtained higher values.

The presence of two Tafel slopes in the anodic polarization curve has been reported by other researchers [32]. Da Silva *et al.* studied Ti supported with IrO_2 (1-x) - Ta_2O_5 (x) with x in the range of 40–55 mol%. Polarization measurements were conducted in a 3 M H_2SO_4 solution in the absence or presence of 0.03 M KPF_6.

In Figure 15, Tafel slopes are presented as a function of different IrO_2 concentrations at various temperatures. The second Tafel slope (b2) depends on the composition of the electrode; it is very sensitive to IrO_2 content in the oxide coating and to temperature.

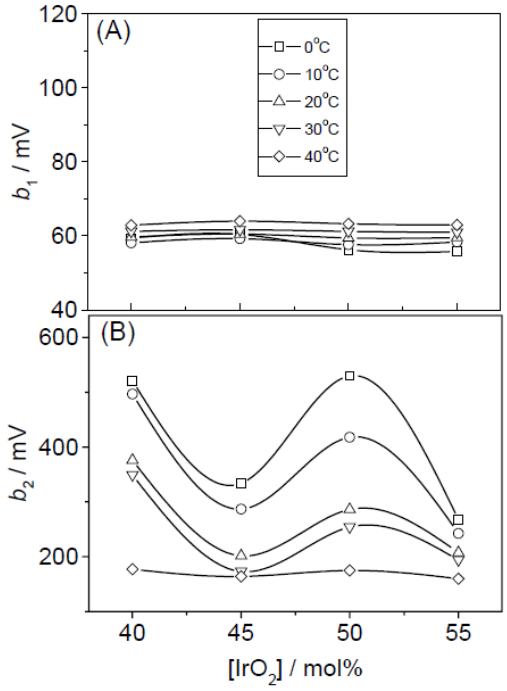

Figure 15. Dependence of the Tafel slope on the electrode composition and temperature for the low (*b*1) and high (*b*2) overpotential domains. Electrolyte: 3 M H_2SO_4 solution [32].

The oxygen evolution reaction on IrO_2–Ta_2O_5 coated Ti electrodes (the nominal compositions of the oxide coatings are 10, 30, 50, 70, and 90 mol% Ir) was investigated by Xu and Scantlebury [23] using potentiodynamic polarization measurements in a 0.5 M Na_2SO_4 solution.

Figure 16 presents the current density as a function of the composition of the oxide coating at constant potential values (1150, 1200, and 1250 mV) picked from the polarization measurements. The data indicate that the maximum electrochemical activity occurs on the electrodes with 50–70 mol% Ir. The difference in the current density for electrodes with various Ir concentrations

increases as the polarization potential increases, suggesting the oxygen evolution reaction becomes more facile with an increase in potential.

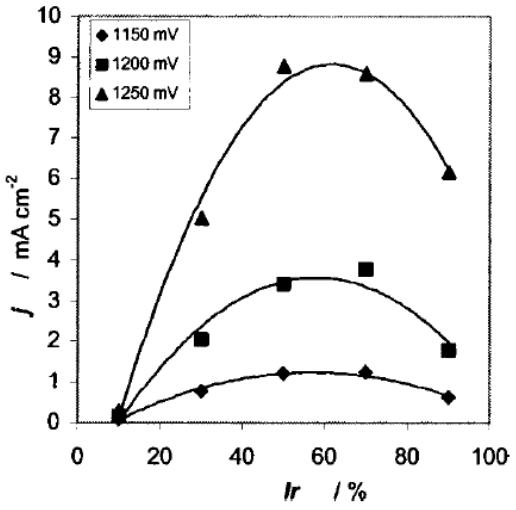

Figure 16. Change in the polarization current density with Ir content in a 0.5 M Na_2SO_4 solution [23].

2.4 Chemical composition analysis and findings on the microstructure of IrO_2-Ta_2O_5 coated Ti electrodes

2.4.1 SEM and energy-dispersive X-ray spectroscopy (EDS) analysis on IrO_2-Ta_2O_5 coated Ti electrodes

2.4.1.1 Findings on fresh and galvanostatically tested electrodes

Studies have been reported on the effect of the chemical composition on the microstructure of iridium oxide−tantalum oxide coatings. The changes in morphology of the IrO_2-Ta_2O_5 (70:30 mol%)–coated Ti electrodes before and after an ALT were studied by Xu *et al*. [20] using SEM

analysis. Typical micrographs are shown in Figure 17. An ALT was carried out in a 1 M sulfuric acid solution at 30°C with an applied current density of 2 A/cm^2.

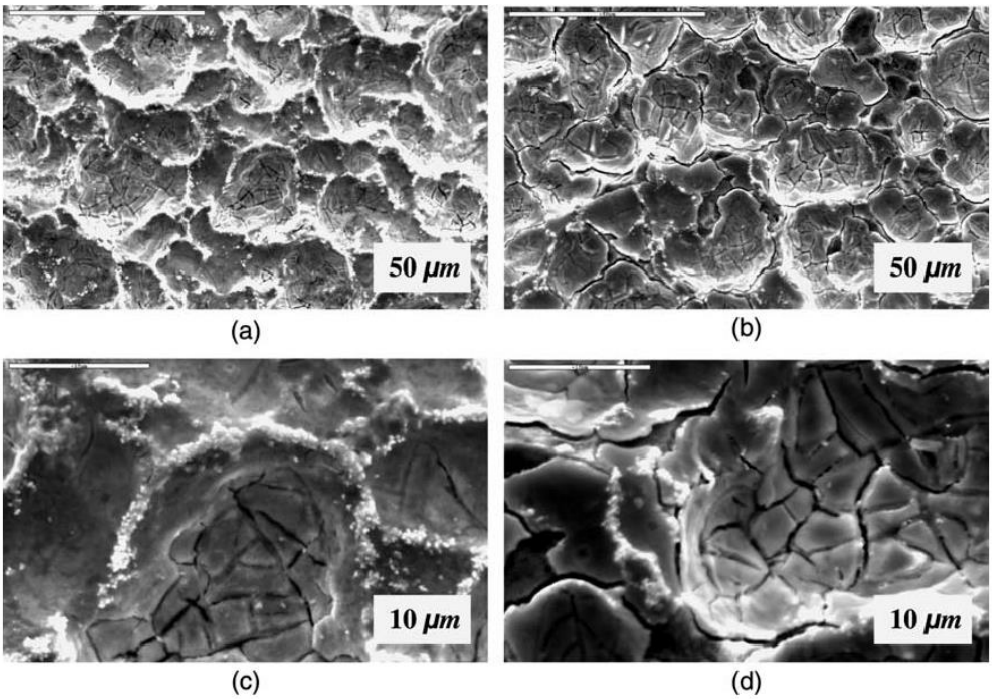

Figure 17. Scanning electron microscope (SEM) micrographs of an IrO_2–Ta_2O_5 anode before (a, c) and after (b, d) an ALT [20].

On the surface of the electrode before the test, the typical morphological features were dried mud–like cracks (~10 μm), agglomerates of particles (~2 μm size), and flat areas (craters). On the electrode subjected to an ALT, the absence of the agglomerates, increasing numbers of cracks, and even some detachment of the oxide coating may be seen. The results of a chemical composition analysis of the different areas performed using an energy-dispersive X-ray spectroscopy (EDS) technique are tabulated in Table 1.

Table 1. Composition of the oxide coating before and after the accelerated lifetime test (ALT) [12]. The ALT was carried out in a 1 M sulfuric acid solution at 30°C with an applied current density of 2 A/cm^2.

Sample	Location	Composition (mol%)		
		Ir	Ta	Ti
Before ALT	Agglomerate	64.41	18.59	17.00
	Flat area	50.44	41.86	7.70
After ALT	Agglomerate	49.92	14.99	35.09
	Flat area	33.31	62.19	4.50
	Detached area	1.36	2.21	96.44

Titanium was detected in the surface analysis even though no Ti was added in the preparation process for the oxide coating. It was concluded that the signal came from the Ti substrate either due to a thinned or delaminated coating. There was no significant change in the ratio of Ir/Ta on the electrodes before and after the ALT; however, the amount of detected Ti increased dramatically after the ALT. This increase, along with the decreasing Ir and Ta detected in the detached area, indicates the removal or thinning of the IrO_2–Ta_2O_5 coatings.

2.4.1.2 Effect of Ti substrate pretreatment on the morphology of IrO_2–Ta_2O_5 electrodes

The effect of pretreatment of the Ti substrate on the properties of the IrO_2-Ta_2O_5 (70:30 mol%)–coated Ti electrodes was investigated by Yan and his coworkers [33]. The traditional way to pretreat Ti substrate is to first degrease it in acetone and then etch it in boiling a 10 wt% oxalic acid solution for 2 hours [20]. This provides uniform roughness of the Ti surface. In their study,

various pretreatments were carried out on the Ti substrates, and then the oxide coating was applied. Field emission scanning electron microscope (FESEM) images of the prepared electrodes are shown in Figure 18.

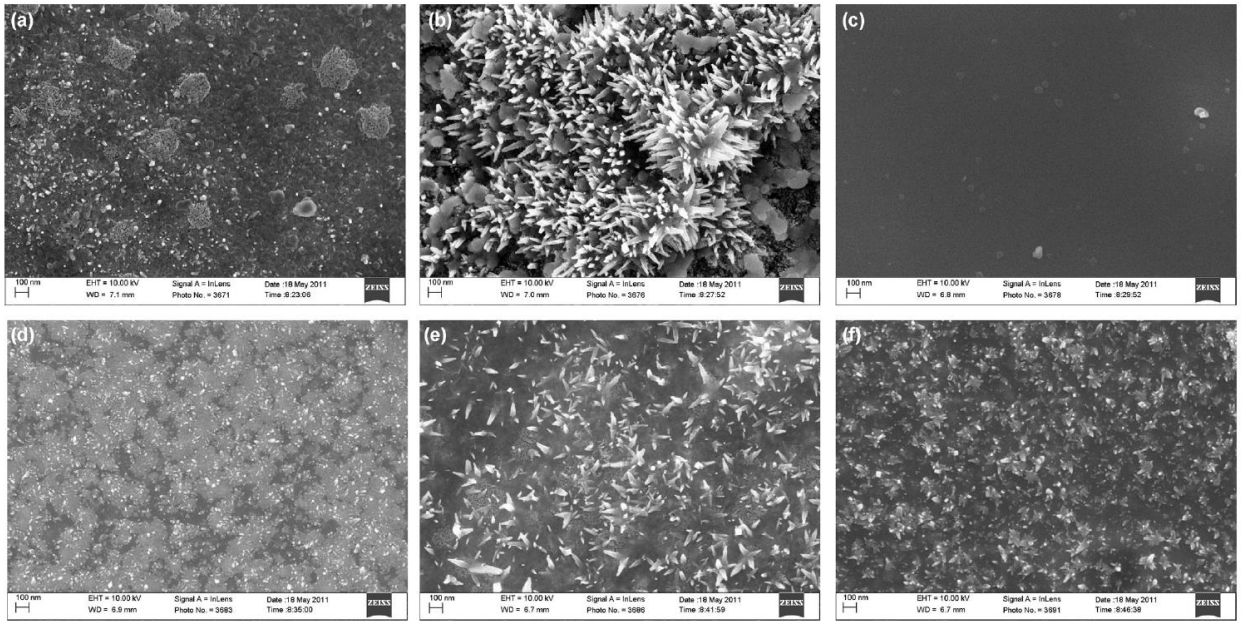

Figure 18. Field emission scanning electron microscope (FESEM) micrographs of IrO_2–Ta_2O_5 anodes (a) untreated substrate, (b) oxalic acid–etched substrate, (c) 300°C hydrogen-treated substrate, (d) 400°C hydrogen-treated substrate, (e) 500°C hydrogen-treated substrate, and (f) 600°C hydrogen-treated substrate [33].

In the FESEM images, all electrodes except the one with the 300°C hydrogen-treated substrate exhibit scattered crystalline IrO_2 agglomerates, which were formed during the preparation process [36]. On the electrode with no pretreatment, the agglomerates (~50 nm in size) appear to be dispersed unevenly. In electrodes formed on a hydrogen-treated substrate, the crystals are relatively larger (~100 nm in size) and more numerous on the substrate subjected to a 500°C hydrogen treatment. Among all of the electrodes, it is evident that the one formed on the oxalic

acid–etched substrate has much larger (~400 nm in size) and more numerous IrO_2 crystals, which is probably due to the rough surface formed in the pretreatment that could promote the crystallization and growth of IrO_2 crystals [35].

A regular SEM analysis was also performed on the electrodes. All samples showed the dried mud−like cracks. The cause of this feature is the quick volatilization of the precursors and the difference in the thermal expansion coefficients of the substrate and the oxide coatings [33]. On the surface of the electrode formed on a substrate that was hydrogen treated at 300°C, peeling of the oxide coating was observed. For the electrodes formed on substrates that was hydrogen treated at 400°C and 500°C, the cracks appear to form connections with one another.

2.4.1.3 Effect of variation in the IrO_2–Ta_2O_5 composition on the morphology of the electrodes

Changes in the morphology of IrO_2–Ta_2O_5 electrodes with nominal IrO_2 contents of 10%, 40%, 60%, 70%, and 90% were studied by Ren *et al.* [36] using SEM analysis. The morphological characterization of the electrodes is provided in Figure 19.

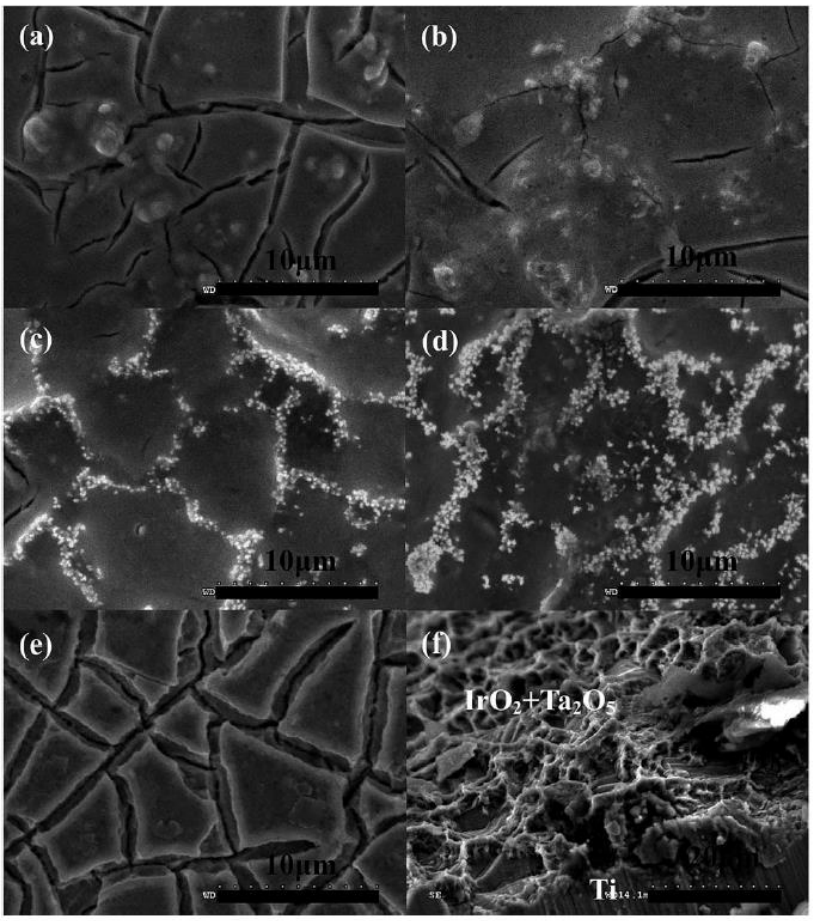

Figure 19. SEM micrographs of Ti/IrO_2–Ta_2O_5 anodes with (a) 10% IrO_2, (b) 40% IrO_2, (c) 60% IrO_2, (d) 70% IrO_2, and (e) 90% IrO_2 and (f) a cross section of the 70% IrO_2 sample [36].

From the SEM micrographs, it is obvious that the typical dried mud–like cracks are present on the surfaces of all electrodes. However, because the content of IrO_2 is different for the different electrodes, changes in the morphology are observed. Crystalline agglomerates/islands increasingly appear on the surface as the amount of IrO_2 increases. Additionally, the agglomerates/islands gradually form a network at the mud crack grain boundaries as the Ir content is increased to 70% IrO_2. From Figure 19f, which is a cross section of the electrode containing 70% IrO_2, the thickness of the oxide coating was estimated to be approximately 150 μm with densely packed crystalline features. On the electrode containing 90% IrO_2, decoration of the (mud) grain boundaries by

crystalline features disappears; perhaps the reason for this is an insufficient amount of tantalum oxide matrix, which is needed for iridium oxide crystallization.

2.4.2 X-ray diffraction (XRD) analysis on IrO_2-Ta_2O_5 coated Ti electrodes

Limited studies have been reported that analyze the crystallinity of Ir-Ta-O coatings prepared by the thermal decomposition method. Ren *et al.* [36] used X-ray diffraction (XRD) analysis to evaluate the changes in the crystalline structure on IrO_2–Ta_2O_5 electrodes with nominal contents of 10%, 40%, 60%, 70%, and 90% IrO_2. The results are displayed in Figure 20. These IrO_2–Ta_2O_5 electrodes were prepared by conventional thermal decomposition, which involves heating to 500°C.

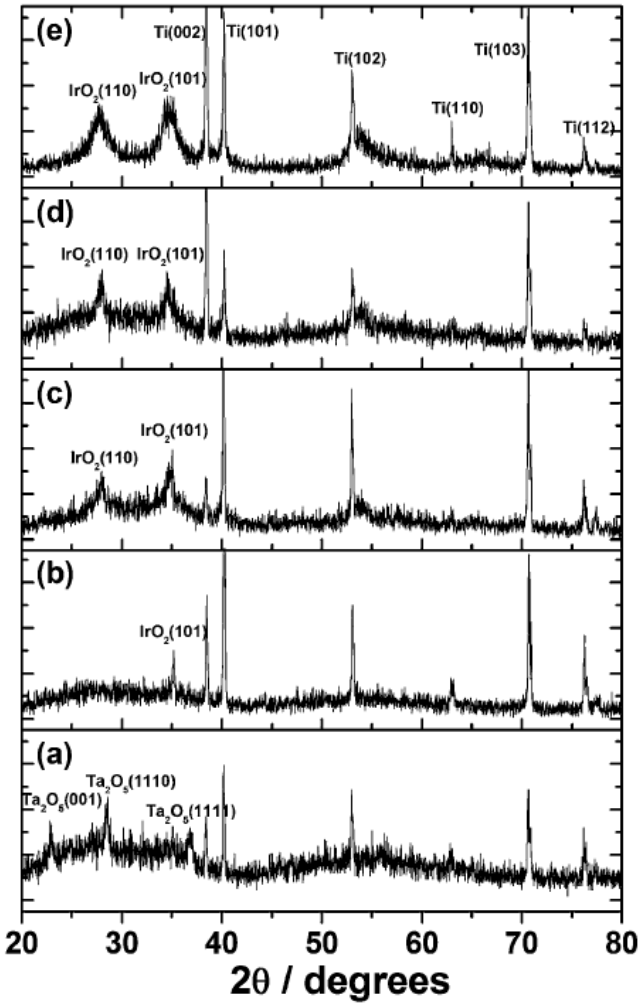

Figure 20. X-ray diffraction (XRD) curves for Ti/IrO_2–Ta_2O_5 anodes with (a) 10% IrO_2, (b) 40% IrO_2, (c) 60% IrO_2, (d) 70% IrO_2, and (e) 90% IrO_2 [36].

The pattern for the coating with 10% IrO_2 indicates the presence of crystalline Ta_2O_5. In the electrodes with 40% IrO_2 or more, diffraction peaks of IrO_2 (rutile type) appear with the disappearance of the peaks of Ta_2O_5. The intensity of the IrO_2 peaks increases with the amount of IrO_2 in the coating. All coatings show the presence of Ti due to the penetration of the X-rays to the substrate [36].

2.4.3 X-ray photoelectron spectroscopy (XPS) findings on IrO_2-Ta_2O_5 coated Ti electrodes

A few studies have been reported on chemical bonding information in IrO_2-Ta_2O_5 coatings prepared by the conventional thermal decomposition method. Composite Ta- and Ir-doped SnO_2 particles were characterized by Ardizzone *et al.* [37] using the XPS technique. The particles were prepared by the sol-gel method at room temperature, beginning with $Sn(C_4H_9O)_4$ and dopant salts of $IrCl_3$x $3H_2O$ (15 mol% Ir) and $TaCl_5$ (7 mol% Ta). The dried xerogels were then heated at 500°C using Ti powder as support. A fresh sample and a sample subjected to a polarization measurement in a 0.1 M $HClO_4$ solution with a 1.4-2 V potential vs. the reversible hydrogen electrode (RHE) at a scan rate of 10 mV/min were characterized using XPS (shown in Figure 21).

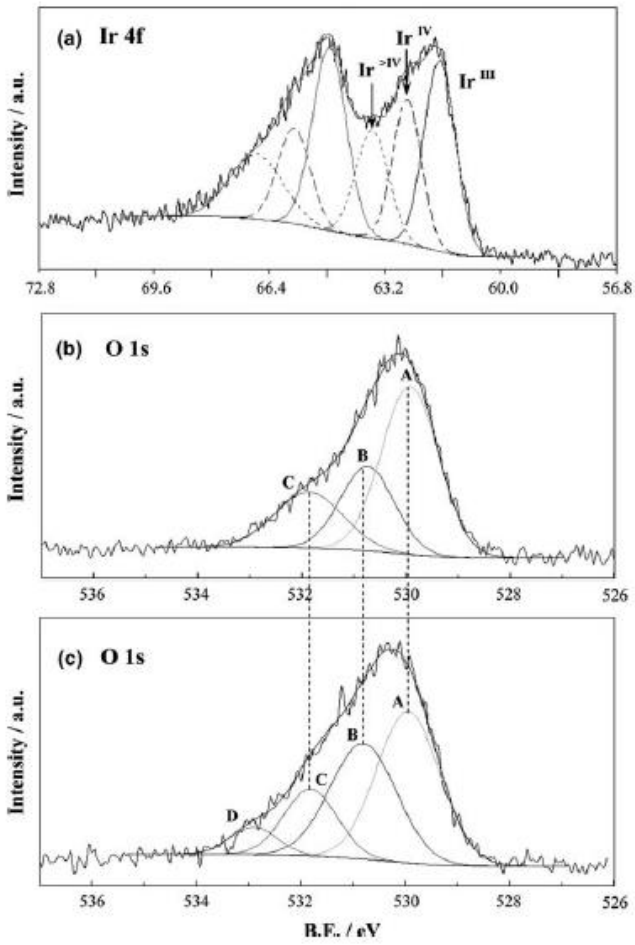

Figure 21. X-ray photoelectron spectroscopy (XPS) spectra of Ti-supported composites (15 mol% Ir): (a) Ir $4f_{7/2,5/2}$ doublets relative to the different Ir spectral components, (b) oxygen 1s peak for a fresh sample, and (c) oxygen 1s peak for the sample subjected to an oxygen evolution reaction in acid media [37].

The Ta 4f peak was barely detected from the samples; therefore, only the peaks for Ir and O are presented. In Figure 21a, the peaks of Ir 4f were fitted using Gaussian lines. From the fitted peaks, three components were identified, which are attributed to Ir (III), Ir (IV), and Ir (higher than IV) at binding energies of 61.7, 62.6, and 63.6 eV, respectively. The authors noted that there was no significant change in the Ir 4f peak shape between the fresh sample and the sample subjected

to the polarization measurement. In Figure 21b, the fitted peaks indicate that three components are present in the fresh sample: lattice oxygen in SnO_2 (component A), hydroxide in $Sn(OH)_4$ or lattice oxygen in IrO_2 (component B), and the OH group in $Ir(OH)_4$ or $IrO(OH)_2$ (component C) at binding energies of 529.9, 530.7, and 531.9 eV, respectively [37]. For the sample subjected to the polarization measurement (Figure 21c), components B and C have larger peaks compared with those from the fresh sample. A new component D also emerges at a higher binding energy (532.9 eV), which is attributed to water.

2.5 Degradation mechanisms

The mechanism of the degradation of the IrO_2-Ta_2O_5 coating in acidic solutions has been studied and reported by Hu *et al.* [16]. They proposed the degradation mechanism model for Ti/ IrO_2-Ta_2O_5 electrodes shown in Figure 22.

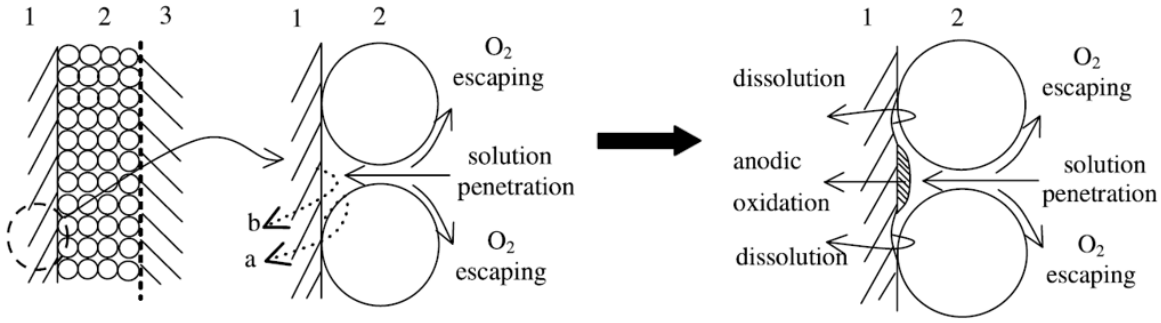

Figure 22. Schematic diagrams for the degradation mechanism model for Ti/IrO_2-Ta_2O_5 anodes. 1-Ti base; 2-oxide catalyst layer; 3-electrolyte. (a) crevice sites; (b) opening sites [16].

As depicted in the schematic diagrams, the electrolyte initially penetrates the IrO_2-Ta_2O_5 coating through pores, reaching portions of the Ti substrate, which causes part of the Ti base to be anodically oxidized. When oxygen is generated on the anode, the electrolyte in the crevice sites

becomes more acidic, and possible dissolution of Ti takes place, creating vacancies in the interface between the oxide coating and the substrate. After a long period of oxygen evolution, some areas of the oxide coating covering the vacancies would peel off, leaving base metal exposed to the electrolyte, which would be further oxidized. As the oxidized Ti layer keeps growing in the exposed regions and at the interface between the coating and the substrate, the resistance of the anode increases, causing a rise in the measured cell potential, suggesting complete failure of the IrO_2-Ta_2O_5 coated Ti electrodes.

In the above reviewed investigations, the accelerated lifetime of thick coatings (many tens of microns) formed on flat titanium samples was tested at an applied current density of 1-2 A/cm^2, which is five to ten times the current density typically used in copper electrowinning. Additionally, none of the studies paid attention to the elucidation of the effect of fluoride ions on lifetime.

In this work, titanium mesh substrates (with 35% open fraction) coated with thin (5-7 microns) oxide films were tested at a much lower current density (0.54 A/cm^2). The effect of fluoride addition to the sulfuric acid baths on lifetime was systematically investigated.

CHAPTER 3

MATERIALS AND EXPERIMENTAL METHODS

3.1 Materials

Electrode samples 8.5 x 2.5 cm in size were procured from a commercial vendor and are shown in Figure 23. The electrode substrate was expanded titanium mesh with an open fraction of 35%. The mesh substrates were greased in acetone and etched in boiling oxalic acid prior to coating to create roughness for better adhesion. Based on the information provided by the vendor, two precursors, H_2IrCl_6 and $TaCl_5$, dissolved in a butanol solution containing a polymeric resin were applied to one side of the substrate by brush coating. Multiple layers were applied: first, four layers were applied and fired at 450°C, then another seven layers were coated and fired at 400°C, producing a total of eleven oxide layers.

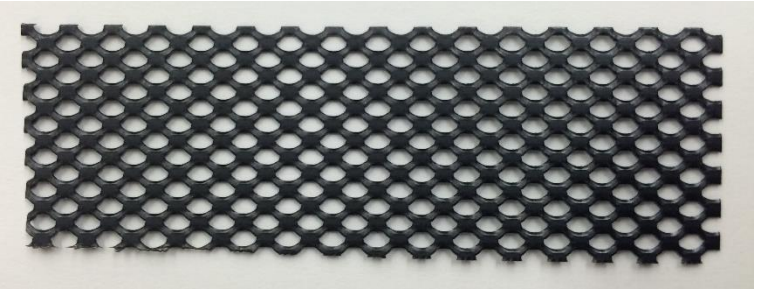

Figure 23. IrO_2-Ta_2O_5 coated Ti expanded mesh electrode.

The chemicals used in this study were sulfuric acid (96%, semiconductor-grade PURANAL™, Sigma-Aldrich), sodium fluoride (>99%, ACS reagent, Acros Organics), aluminum sulfate hexadecahydrate (>95%, ACS grade, VWR), iron (III) sulfate pentahydrate

(>97%, ACS grade, Acros Organics), potassium hydroxide (45 wt%, Fisher Chemicals), and phenolphthalein indicator solution (1% phenolphthalein in 39.3% isopropanol, Fisher Chemicals).

3.2 Electrochemical measurements

3.2.1 Accelerated lifetime test (ALT)

Generally, the service life of IrO_2-Ta_2O_5 coated Ti electrodes is expected be 2–3 years. Therefore, to evaluate the lifetime of the electrode within a much shorter time period, it is necessary to use the accelerated electrochemical technique described in Chapter 2—the ALT. An ALT is a galvanostatic method in which a constant current density is applied to the anode, and the changes in the cell potential between the anode and cathode are monitored. The experimental setup for an ALT is provided in Figure 24.

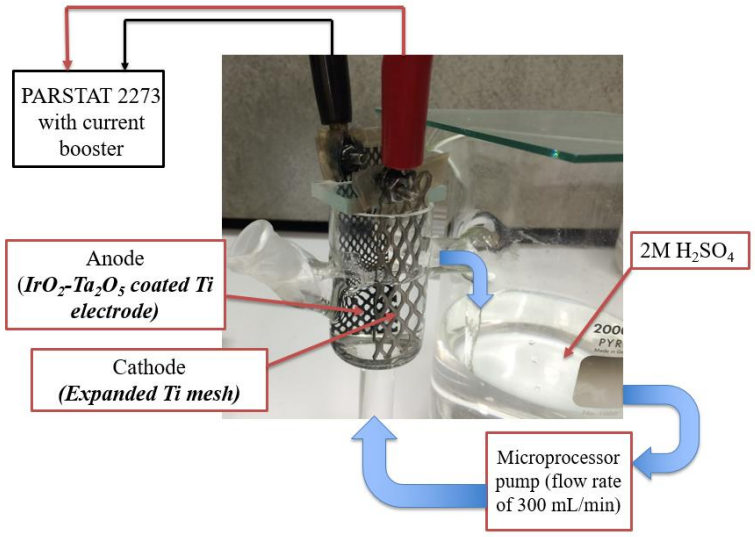

Figure 24. Experimental setup for an accelerated lifetime test.

ALTs were carried out in a customized electrochemical cell, shown in Figure 32. In the cell (50 mL), an IrO_2-Ta_2O_5 coated Ti electrode was used as the anode, and a bare Ti mesh was

used as the cathode. The oxide-coated side of the anode was placed facing the cathode. During the ALT, the electrolyte—a 2 M sulfuric acid solution at ambient temperature—was pumped at a flow rate of 300 mL/min by a microprocessor pump and recirculated during the entire measurement. A glass plate was used to cover the top of the beaker to prevent water evaporation, and a small glass piece was placed between the anode and the cathode to minimize acid mist corrosion of the electrical contacts. For the ALTs involving fluoride addition, a polypropylene cell was used. A constant current density of 0.54 A/cm^2 was applied to the anode by PARSTAT 2273 coupled with a KEPCO current booster. The changes in cell potential were recorded using the software PowerSuite®. Every 16 minutes, one data point was collected.

The test solutions were 2 M sulfuric acid solutions (without any copper ions) in the absence and presence of fluoride (25, 100, and 200 ppm) added as sodium fluoride. In tests aimed at determining the effect of fluoride complexation by metal cations such as aluminum and ferric ions on anode life, pre-calculated amounts of aluminum sulfate or ferric sulfate were added to the test solution.

During the ALT, titrations were carried out once every two days to determine water loss due to decomposition to oxygen at the anode and thereby estimate the amount of water to add to keep the sulfuric acid concentration at the required level. Each time, 5 mL of test solution was taken and then diluted to 100 mL. This acidic solution was then titrated with 1M KOH solution using a burette. Phenolphthalein was used as the indicator. The endpoint of titration was when the pink/purple color remained for at least 15 seconds. An example of the calculation on the amount of water added based on the titration data is described below.

If the volume of 1 M KOH used to neutralize the diluted acid solution is 22.4 mL, the number of moles of KOH used is $0.0224\ moles$ ($\frac{22.4}{1000} L \times 1\ \frac{mole}{L}$). Based on the chemical reaction shown in Equation 3.1, the amount of H_2SO_4 in diluted solution is calculated to be 0.0112 moles.

$$H_2SO_4 + 2\ KOH \rightarrow K_2SO_4 + 2\ H_2O \tag{3.1}$$

Under this condition, the concentration of sulfuric acid in the test solution is 2.24 M ($\frac{0.0112}{0.1} \times 20\ M$).To bring the sulfuric acid back to the original concentration, 107 mL ($1L - \frac{1L \times 2M}{2.24\ M}$)of water had to be added.

Typical concentration of sulfuric acid in the solutions were in the range of 2.1-2.4 M, requiring the addition of roughly 45-165 mL of water every two days.

3.2.2 Anodic polarization measurements

An anodic polarization measurement is a simple and rapid way to study changes in the overpotential for the oxygen evolution reaction on the electrodes before and after ALTs. Measurements were performed in a three-electrode system by setting one electrode as the working electrode, a Pt foil as the counter electrode, and a saturated calomel electrode (SCE) as the reference electrode in 2 M sulfuric acid solutions. Measurements were carried out by polarizing the electrode from 1 to 2 V vs. SCE at a scan rate of 2 mV/s. From the polarization measurement results, the overpotential for oxygen evolution was calculated.

3.3 Speciation calculations

Speciation calculations were carried out using the computer software STABCAL. The input parameters are species with corresponding valence, concentration, solution potential range,

solution pH range, ionic strength, and activity model. A personal database was created from three available databases—NBS, Minteq, and Critical.

Depending on the ionic strength of the medium, the activity coefficients of the ions can be calculated according to one of three different models, which are given below.

Model 1: Davies equation for ionic strength (I) less than 0.5 M.

$$log\gamma_i = -Az^2(\frac{\sqrt{I}}{1+\sqrt{I}} - 0.3I)$$

where $A = 1.82\times 10^6(\varepsilon T)^{-3/2}$ (ε is dielectric constant).

Model 2: Specific interaction theory equation, used for $0.5\ M < I < 5\ M$.

$$log\gamma_i = -Az^2\frac{\sqrt{I}}{1+1.5\sqrt{I}} + \sum_i \epsilon(i,j)m_j$$

where $A = 1.82\times 10^6(\varepsilon T)^{-3/2}$ (ε is the dielectric constant) and ϵ is the coefficient of ionic interaction from the ion pair of i and j.

Model 3: Extended Debye-Huckel equation for $I < 0.1\ M$.

$$log\gamma_i = -Az^2(\frac{\sqrt{I}}{1+Ba\sqrt{I}})$$

where $A = 1.82\times 10^6(\varepsilon T)^{-3/2}$ (ε is the dielectric constant), $B = 50.2904(\varepsilon T)^{-1/2}$, and *a* is the size of the ion.

In this work, the test solutions are 2 M sulfuric acid solutions containing various levels of fluoride. The ionic strength of 2 M sulfuric acid was calculated as follows:

$$I = \frac{1}{2}(\sum C_i Z_i^2) = \frac{1}{2}[(4\ M)\times(1^2) + (2\ M)\times(-2)^2] = 6\ M$$

This ionic strength of 6 M is beyond the suggested ranges covered by the three activity models; only the range used in model #2 is relatively close. Therefore, activity model #2 (specific interaction theory equation) was used in this work. It is important to point out that the activity model #2 is developed on a 5 M KCl solution. The ionic strength of the electrolyte used in testing is 6 M and this might subject to some inaccuracy. Specific species considered in the calculation are listed in the Appendix A.

3.4 Microstructure and chemical composition analysis

The morphology and chemical composition of the oxide coating were characterized using a variable pressure scanning electron microscope (VPSEM, Hitachi S-3400). The microstructure and elemental analysis were performed at a 30 keV accelerating voltage. The coating structure was characterized by an X-ray diffraction (XRD) analysis on a PANalytical X'pert Plus instrument equipped with a programmable incident beam slit and an X'Celerator detector. The X-ray radiation was Cu Kα with a λ of 1.5418 Å.

The surface chemical composition and chemical bonding information were analyzed using X-ray photoelectron spectroscopy (XPS), which was performed with a Kratos Axis 165 Ultra X-ray photoelectron spectrometer equipped with a monochromatized Al-Kα X-ray source (energy of 1486.6 eV). Curves for the elements (Ir, Ta, and O) were fitted using Gaussian and Lorentzian functions.

Samples of the test solutions were collected every two days during the ALT for analysis of the dissolved elements (Ir and Ta) using inductively coupled plasma mass spectrometry (ICP-MS) (ELAN DRC II ICP Mass Spectrometer).

CHAPTER 4

RESULTS AND DISCUSSION

4.1 Effect of fluoride addition to sulfuric acid solutions on the lifetime of IrO_2-Ta_2O_5 coated Ti mesh electrodes

4.1.1 X-ray diffraction analysis of a fresh electrode

X-ray diffraction (XRD) was used to characterize the crystalline structure of IrO_2-Ta_2O_5 coating on Ti mesh. The diffraction pattern of a fresh (unused) electrode is shown in Figure 25.

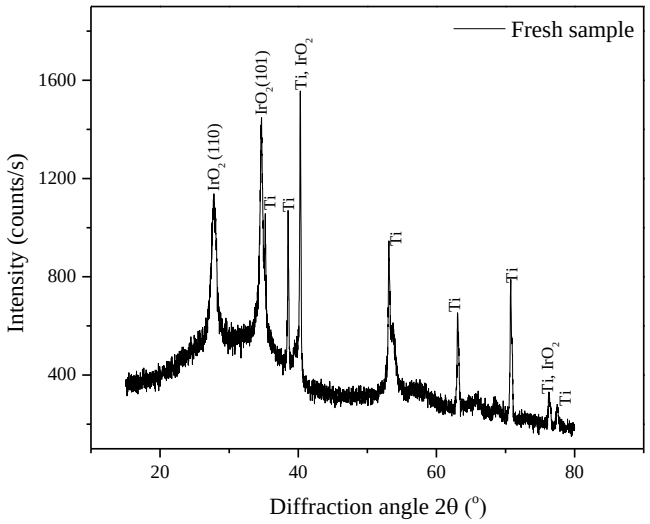

Figure 25. XRD pattern of the IrO_2-Ta_2O_5 coating on Ti mesh.

The diffraction pattern contains reflections characteristic of two materials, Ti and IrO_2. The peaks at 2θ values of 27.7 and 34.7 degrees may be assigned to the (110) and (101) orientations of

the IrO_2 rutile phase in the coating [36]. No characteristic peaks for Ta_2O_5 were detected, indicating the absence of Ta_2O_5 crystallization of during the thermal treatment of the coating.

4.1.2 Coating thickness determination

Two virgin anode samples were mounted in epoxy with the oxide coating sides facing one another and hand polished with 400, 600, 800, and 1200 grit sand-paper to reveal the cross section of the samples (Figure 26a). A SEM image of the cross-section of one of the samples at a magnification of 1000 x is shown in Figure 26b. In the image, the white band indicates the IrO_2-Ta_2O_5 coating, which is clearly not uniform and varies in thickness. To estimate the thickness of the coating, elemental maps of Ir, Ta, and Ti were obtained using EDS analysis (Figure 27). From the emission spectrum region that is strongly associated with Ir and Ta signals, the coating thickness was estimated to be in the range of 4.8 to 6.9 µm. The strong titanium signal is due to the underlying Ti mesh.

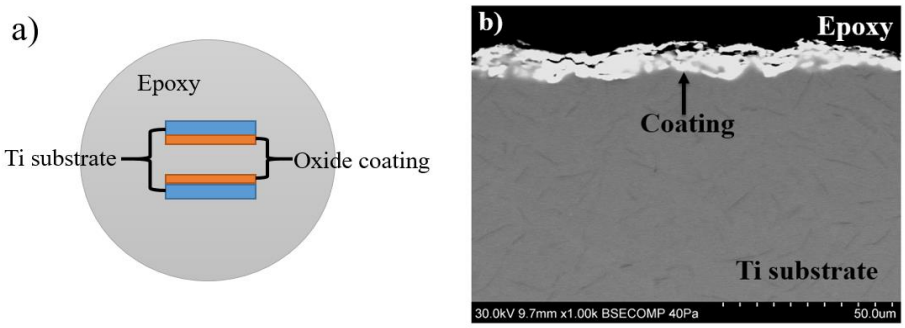

Figure 26. A schematic of the mounted samples (a). A SEM image of the oxide coating on a Ti substrate at a magnification of 1000 x (b) [courtesy of Vanda Ngo, Master's student, University of Arizona].

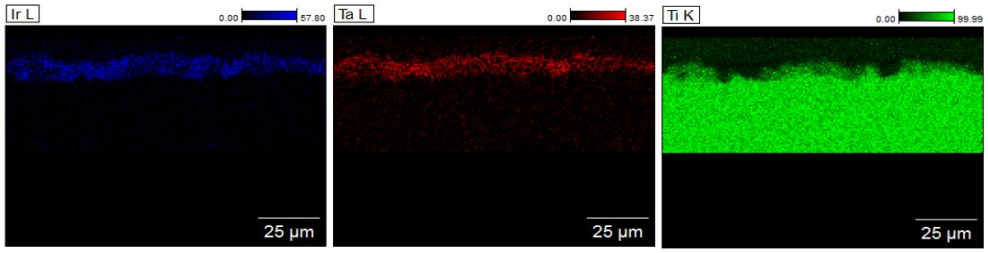

Figure 27. Elemental maps of Ir, Ta, and Ti generated from the EDS analysis (courtesy of Vanda Ngo).

4.1.3 Results of accelerated life test (ALT)

A representative plot of the data from an ALT is shown in Figure 28. This particular test was carried out in a solution containing 25 ppm fluoride. When the current is turned on, the cell potential instantly jumps to ~ 5 V. The potential remains roughly constant until 550 hours and then begins to rise slowly. The point at which the potential reaches a value that is 5 V larger than the constant potential value is defined as the accelerated lifetime.

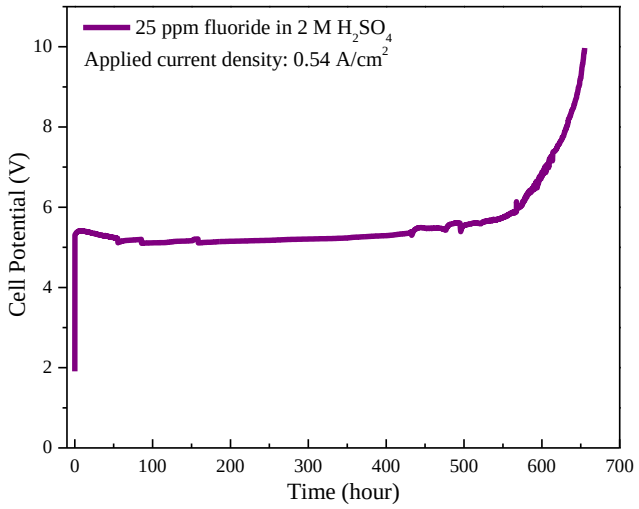

Figure 28. Measured cell potential as a function of ALT time in a 2 M H_2SO_4 solution containing 25 ppm fluoride.

Figure 29 provides plots of the measured cell potential as a function of ALT time in the absence and presence of various levels of fluoride in 2 M H_2SO_4 solutions. As can be seen from the data in this figure, the accelerated lifetime is quite long (more than 500 hours) in the absence of any added fluoride. The lifetime decreases as fluoride content increases and is approximately 110 hours at an added fluoride concentration of 200 ppm.

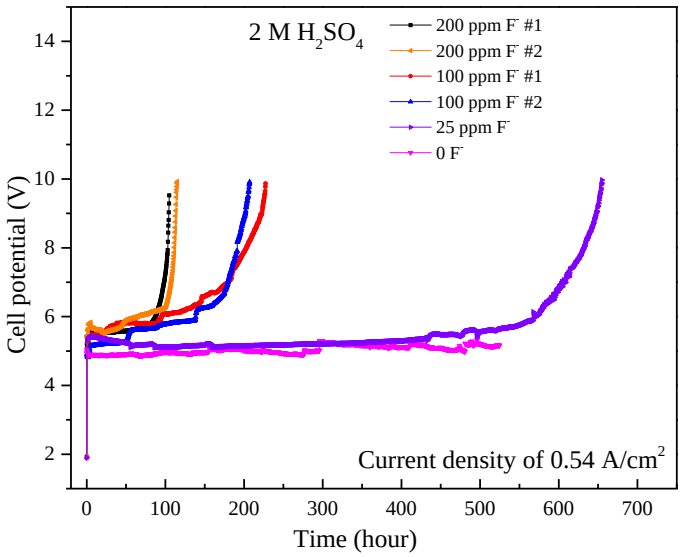

Figure 29. Plots of cell potential vs. ALT time in 2 M H_2SO_4 solutions in the absence and presence of added fluoride ions.

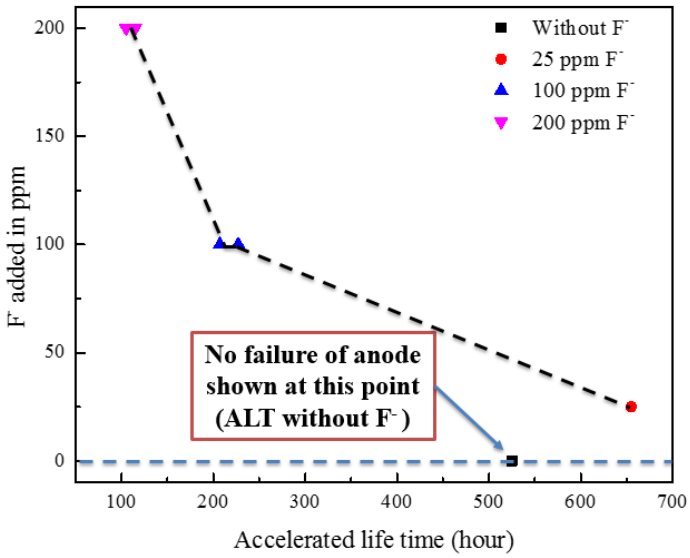

Figure 30. Accelerated lifetime as a function of fluoride added to 2 M sulfuric acid solution.

The results of ALTs carried out in sulfuric acid solutions in the absence and presence of fluoride ions are summarized in Figure 30. The accelerated lifetime of the electrode is strongly dependent on the level of added fluoride. Higher levels of fluoride result in shorter lifetimes. For example, electrodes failed after ALTs in sulfuric acid solutions containing 200 ppm fluoride for ~100 hours. When fluoride level decreased to 25 ppm, the electrode failed after ~650 hours.

4.1.4 Anodic polarization measurements

The anodic polarization behaviors of the IrO_2-Ta_2O_5 coated Ti mesh anodes before and after ALTs were measured in 2 M H_2SO_4 solutions at a sweep rate of 2 mV/s. The polarization curves (after iR compensation correction) are given in Figure 31.

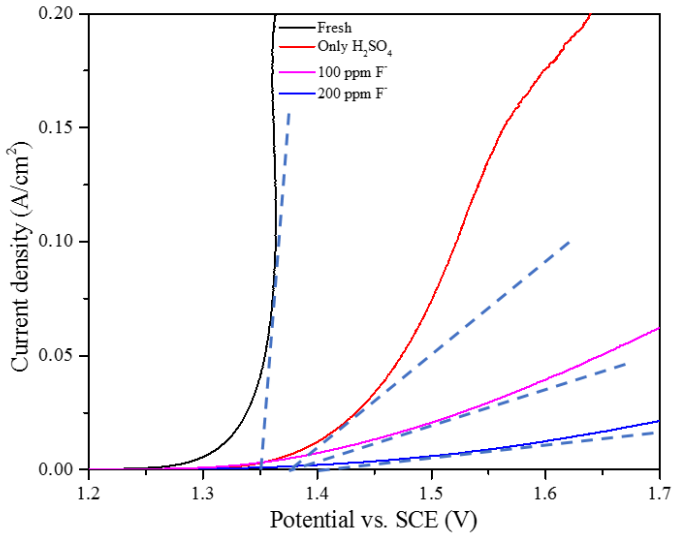

Figure 31. Anodic polarization curves (after iR compensation correction) of IrO_2-Ta_2O_5 coated Ti mesh electrodes in 2 M sulfuric acid solutions: fresh sample and samples after ALTs.

The overpotential for oxygen evolution (η_{O_2}) is calculated using the Equation (2.6) in Chapter 2 and listed in Table 2.

Table 2. Overpotential for oxygen evolution (average values presented from multiple measurements in 2 M sulfuric acid solutions).

Anode Sample	**Overpotential**
Fresh	0.33±0.01 V
After ALT in H_2SO_4	0.35±0.02 V
After ALT in H_2SO_4 with 100 ppm fluoride	0.35±0.01 V
After ALT in H_2SO_4 with 200 ppm fluoride	0.38±0.01 V

Table 2 demonstrates that there are no significant changes in overpotential for oxygen evolution. However, current density decreases at all overpotential values after ALTs, regardless of absence or presence of fluoride or aluminum addition.

As depicted in Figure 31, the measured current density decreases at 1.4 V vs. SCE on electrodes after ALTs in solutions with high levels of fluoride, suggesting that it becomes more difficult for the oxygen evolution reaction to occur on electrodes under these conditions. Clearly, the electrocatalytic performance of electrodes is greatly inhibited when subjected to galvanostatic testing in fluoride-containing solutions.

4.1.5 SEM and EDS analysis

The morphology of IrO_2-Ta_2O_5 coatings before and after ALTs is shown in Figure 32. The oxide coating on a fresh anode consists of "dried-mud" cracks [2, 33], amorphous phases, and crystalline phases. The crystalline phases are precipitated IrO_2 crystallites (agglomerates), which agrees with findings reported in the literature [19, 20, 38]; this finding was confirmed by an EDS point-and-shoot analysis.

Complete removal of the coating, deep cracks, scattered agglomerates on the edge of the crack, and localized thinning are clearly seen on the surface after being subjected to galvanostatic conditioning in 2 M H_2SO_4 for 525 hours. For the anode after an ALT in 2 M H_2SO_4 with 100 ppm fluoride for 207 hours, more of the coating is removed, and cracks are formed on the surface with scattered agglomerates. On the anode after an ALT in 2 M H_2SO_4 with 200 ppm fluoride for 105 hours, almost all agglomerates disappear and large areas of the coating are detached. Jagged features are even observed in some areas after removal of the oxide coating. In an EDS analysis of the jagged areas, only Ti is detected (no Ta or Ir), suggesting that complete removal of the oxide coating took place and that the Ti mesh substrate was exposed to the electrolyte. As seen in Figure

32 (a) to (d), the stability of the IrO_2-Ta_2O_5 coating decreased dramatically due to the presence of fluoride; even the anode substrate seems to be attacked in solutions containing higher fluoride levels.

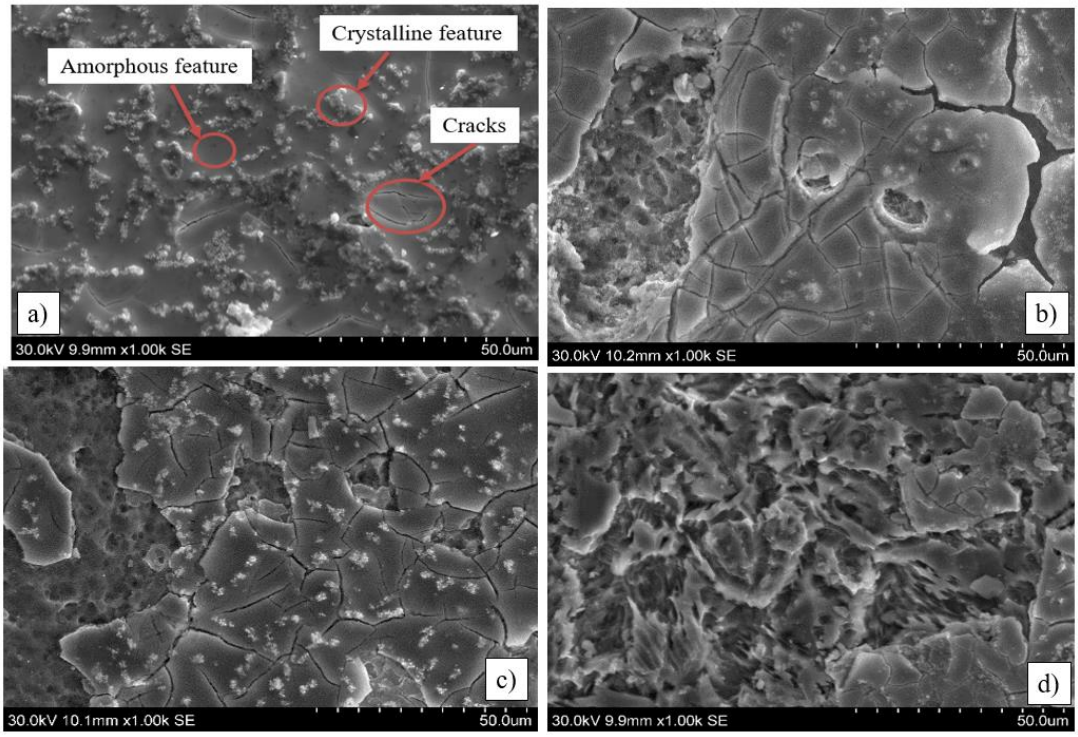

Figure 32. SEM images (magnification 1000 x) of IrO_2-Ta_2O_5 coated anodes before and after ALTs (a–fresh anode, b–anode after an ALT in 2 M H_2SO_4 for 525 hours, c–anode after an ALT in 2 M H_2SO_4 with 100 ppm fluoride for 207 hours, and d–anode after an ALT in 2 M H_2SO_4 with 200 ppm fluoride for 105 hours) (Vanda Ngo assisted in the SEM analysis).

The chemical composition of the anode surface/sub-surface regions before and after ALTs analyzed by EDS is listed in Table 3. Although Ti is not present in the precursors used to prepare the oxide coating, a Ti signal was detected in the surface analysis. Because the oxide coating is thin and not uniform, the Ti signal probably resulted from the penetration of electrons into the substrate. The composition of the oxide coating on the fresh anode, ignoring the Ti signal, can be calculated to be ~70 mol% IrO_2 and 30 mol% Ta_2O_5. On the anode sample after an ALT in 2 M

H_2SO_4 without fluoride, the detected amounts of both Ta and Ir are reduced, but there seems to be a slight preferential dissolution of Ir [20]. Consequently, the molar ratio of IrO_2 to Ta_2O_5 is decreased from the original value. On the electrode sample after an ALT in the 100 ppm fluoride–containing solution, less Ir and Ta is present, while more Ti is detected on the surface. After an ALT in the 200 ppm fluoride–containing solution, the amount of Ta and Ir detected is significantly decreased, with a concomitant increase in the Ti signal. It is interesting that the molar ratio of IrO_2 to Ta_2O_5 is not very far from that of the virgin sample. This suggests coating removal, and/or localized thinning.

Table 3**.** Anode coating composition before and after ALTs.

	Average Mol%			
Element	Fresh Anode	Anode After ALT in H_2SO_4 with 0 ppm F	Anode After ALT in H_2SO_4 with 100 ppm F	Anode After ALT in H_2SO_4 with 200 ppm F
Ta/Ta_2O_5	22.32/28.7	15.74/35.61	14.99/37.67	5.05/24.15
Ir/IrO_2	27.74/71.3	14.23/64.39	12.4/62.33	7.93/75.85
Ti	49.94	70.03	72.61	87.02

4.1.6 ICP-MS analysis

During ALTs, solution samples (5 mL) were collected every two days for ICP-MS analysis of the dissolved elements. Figure 33 shows the concentration of Ta and Ir in solution as a function of ALT time vs. time in 2 M H_2SO_4 solution with 200 ppm fluoride. Also plotted in this figure is the cell potential as a function of time.

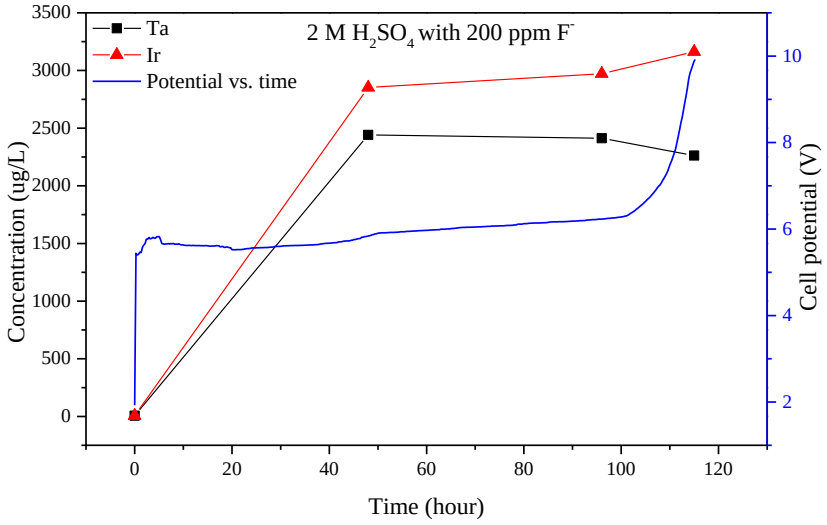

Figure 33. Concentration of Ta and Ir elements vs. time and cell potential for an ALT in 2 M H_2SO_4 solution with 200 ppm fluoride.

The concentration of both elements rise in the first 48 hours of the ALT, but after that point, they remain relatively constant until the end of the test. The common trend in the Ta and Ir concentrations indicates that the oxide coating lost both IrO_2 and Ta_2O_5 in the first 48 hours. It is interesting that continued dissolution does not occur, indicating some sort of equilibrium between the coating and the solution has been reached. The IrO_2–to–Ta_2O_5 ratio of the plateau concentrations is roughly 70 mol% IrO_2 to 30 mol% Ta_2O_5, which is almost the same as the ratio in the coating. This indicates stoichiometric dissolution during the ALT.

4.1.7 Potential-pH diagrams

The potential-pH diagrams of Ta-H_2SO_4-F and Ir-H_2SO_4-F systems are shown in Figure 34. Calculations were performed under conditions of 0.0001 M Ta or Ir in 2 M H_2SO_4 with 200 ppm fluoride using the STABCAL program. It is important to point out that the activity model #2 is developed on a 5 M KCl solution. The ionic strength of the electrolyte used in testing is 6 M and

this might subject to some inaccuracy. Specific species considered in the calculation are listed in the Appendix A.

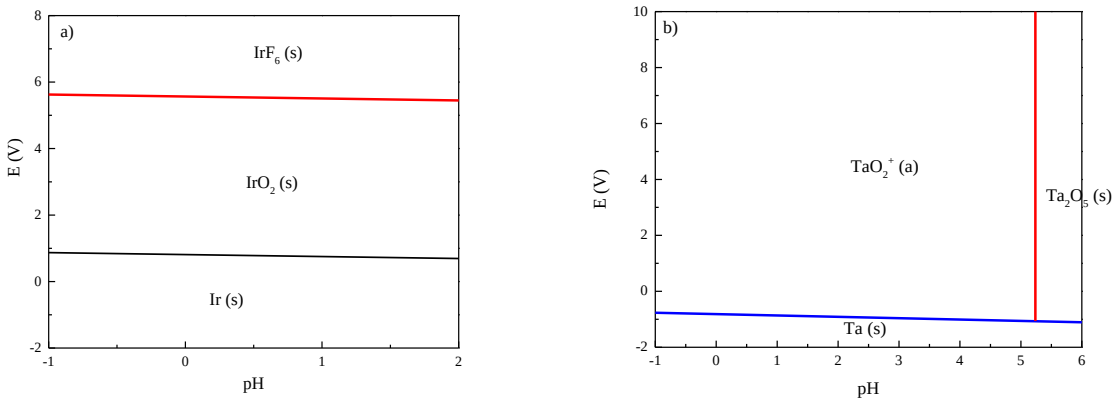

Figure 34. Pourbaix diagrams for Ir-H_2SO_4-F (a) and Ta-H_2SO_4-F (b) systems in 2 M H_2SO_4 (pH of ~ -0.54) with 200 ppm fluoride. Ir and Ta ions both have the same concentrations of 0.0001 M.

From Figure 34, in the Ir-H_2SO_4-F system, solid IrO_2 is the thermodynamically favorable species when the potential is above 1 V at a pH of -0.54. When the potential increases above 6 V, solid IrF_6 becomes the dominant species. The formation of IrF_6 is caused by the presence of HF and its attack on the IrO_2 component.

In the Ta-H_2SO_4-F system, even though fluoride complexes of Ta (TaF_5, TaF_6^-, and TaF_7^{2-}) were considered in the calculations, the most stable specie is aqueous TaO_2^+ when the potential is above 0 V. This implies that fluoride does not play a role in the dissolution of the Ta_2O_5 component.

4.1.8 Speciation calculations for sulfuric acid solutions containing fluoride

Speciation calculations were carried out using the computer software STABCAL to predict thermodynamically favorable species in 2 M sulfuric acid solutions containing added fluoride (referred to as total fluoride or F_T). The selected activity model is #2 (specific interaction theory equation) as discussed in Chapter 3.

The results of the calculations done for different values of total amount of fluoride added (F_T) are shown in Table 4. In 2 M sulfuric acid solutions (pH of ~ -0.54) containing 10 ppm of F_T, 99.7% of the added fluoride is predicted to be in the form of HF. At higher values of F_T (100 to 200 ppm), a small amount of other fluoride species such as H_2F_2 and HF_2^- is predicted to exist in solution.

Table 4. Percentage of various fluoride species in 2 M H_2SO_4 (pH of ~-0.54) solution containing different levels of added fluoride.

Total Fluoride Added	**Percentage**			
	HF	**F^-**	**H_2F_2**	**HF_2^-**
10 ppm	99.7	0.02	0	0
25 ppm	99.2	0.02	0	0
100 ppm	97.1	0.02	2.8	0.004
200 ppm	94.6	0.02	5.3	0.008

4.1.9 Degradation mechanism

Based on the results of the electrochemical studies and microstructure analysis described above, a degradation mechanism for IrO_2-Ta_2O_5 coatings in 2 M H_2SO_4 solutions with fluoride addition is proposed. The deactivation mechanism of the IrO_2-Ta_2O_5 coated Ti mesh electrode under galvanostatic conditions may be generally attributed to detachment of the loosely attached components of the IrO_2-Ta_2O_5 coating due to oxygen evolution, electrochemical dissolution of the active components of the coating, and the formation of a passivation layer on the substrate [30]. Because the differences in the morphology of the different electrode samples are not very significant, the cause of the differences in anode stability during ALTs is the varying compositions of the selected test solutions. The chemical reactions that are likely to take place during ALTs in fluoride-containing solutions are as follows:

$$F^- + H^+ \rightarrow HF \qquad \text{(in solution)} \qquad (4.3)$$

$$6HF + IrO_2(s) \rightarrow IrF_6(s) + 2H_2O + H_2 \uparrow \qquad (4.4)$$

$$Ta_2O_5 + 2H^+ \rightarrow 2TaO_2^+ + H_2O \qquad (4.5)$$

When fluoride is added as NaF into a 2 M H_2SO_4 solution, HF (pKa of 3) is the dominant fluoride-containing species. The HF starts attacking the cracks on the coating surface and travels deeper as the test solution penetrates these cracks. The active component IrO_2 would be attacked by HF to form IrF_6 species, while Ta_2O_5 reacts with acid in solution to form TaO_2^+ species. Meanwhile, gas bubbles are constantly generated on the coating surface, causing spalling. The congruent electrochemical dissolution and spalling of the oxide coating results in complete removal of the coating and exposure of the Ti mesh substrate to 2 M H_2SO_4 solutions with fluoride addition. In this way, the formation of a passivation layer of Ti is accelerated, causing a rise in cell voltage and shortening the anode lifetime.

4.2 Development of a strategy for extending the lifetime of electrodes in fluoride-containing solutions

4.2.1 Effect of aluminum addition to sulfuric acid solutions containing fluoride on lifetime of electrode

Because it is well known that HF can attack iridium and tantalum oxides [39], one approach to improving the lifetime of iridium-tantalum oxide electrodes in sulfuric acid solutions containing fluoride is to reduce the fluoride level by complexation. When metallic cations such as aluminum ions are introduced into sulfuric acid solutions containing fluoride, they may complex both fluoride and sulfate ions. Figure 35 depicts the distribution of various aluminum species upon the addition

of 2800 ppm (0.1053 M) Al^{3+} ions to a 2 M sulfuric acid solution containing 100 ppm of total fluoride. At a pH of -0.54, 80% of the added aluminum is complexed by sulfate as $AlSO_4^+$ and $Al(SO_4)_2^-$ and 5% is complexed by fluoride as AlF^{2+}. From the data in this figure, it can be estimated that the binding of fluoride by aluminum ions will reduce the free fluoride (total fluoride minus complexed fluoride) level to 4 ppm. At this free fluoride concentration, the HF concentration was calculated to be 4.3 ppm. Thus, the addition of 2800 ppm (0.1053 M) aluminum ions to a 2 M sulfuric acid solution containing 100 ppm added fluoride (aluminum-to-fluoride ratio of 20:1) greatly decreases the HF concentration.

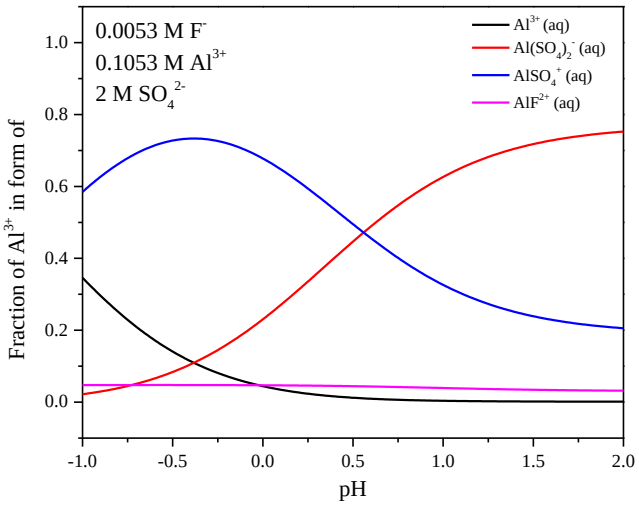

Figure 35. Fraction of Al^{3+} present in the form of different species in a sulfuric acid solution containing aluminum and fluoride ions (molar ratio of Al^{3+} to F^- is 20:1).

Calculations were also performed for other molar ratios of Al to F, and the results are displayed in Figure 36. As is evident from this figure, the higher the Al/F ratio, the lower the amount of HF in the solution. Based on these results, a ratio of 20:1 was used to test the effectiveness of aluminum ion addition at increasing the time to failure in ALTs.

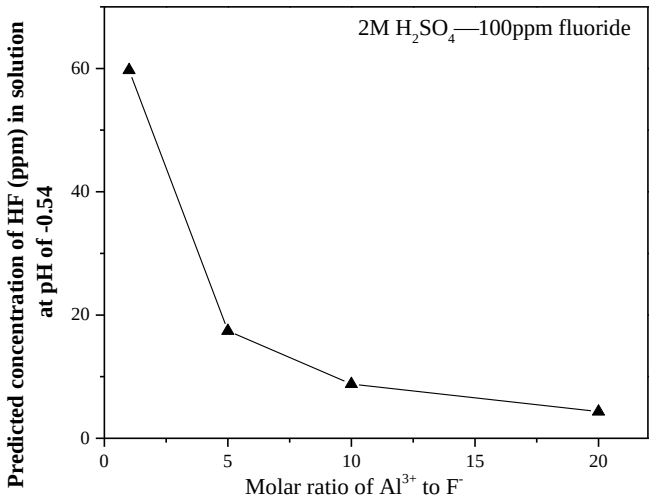

Figure 36. Predicted concentration of HF at various molar ratios of Al^{3+} to F^- for a total fluoride level of 100 ppm.

An ALT was carried out to verify the speciation calculations using the molar ratio of Al to F of 20:1 in sulfuric acid solutions and the result is shown in Figure 37. Upon the addition of aluminum ions to a 100 ppm fluoride solution, the lifetime of the electrode was increased from ~ 250 hours to more than 500 hours. This increase in lifetime is clearly due to a reduction in HF resulting from complexation of the added fluoride by aluminum ions.

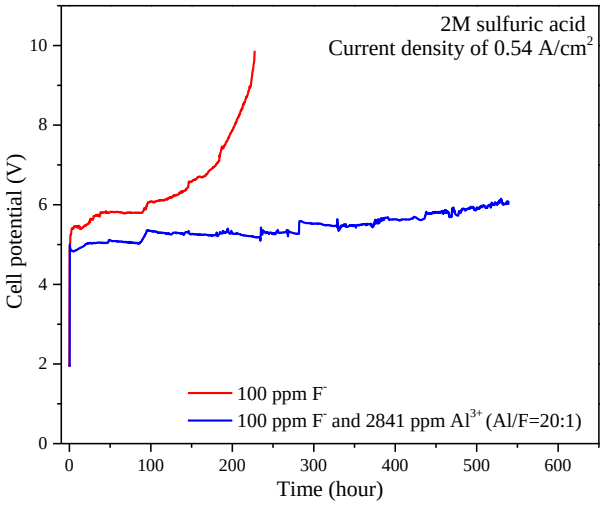

Figure 37. Comparison of ALTs in sulfuric acid solutions containing 100 ppm fluoride with an applied current density of 0.54 A/cm^2 in the absence and presence of aluminum ions.

4.2.1.1 XPS analysis

Chemical bonding information in IrO_2-Ta_2O_5 coating was explored using XPS analysis. The XPS spectrum for Ir, Ta and O in the as-received as well as galvanostatically stressed samples are presented in Figure 38 (a), (b), and (c). The binding energy values and intensities obtained based from height of Ir 4f, Ta 4f and O1s peaks are tabulated in Table 5 and 6, respectively.

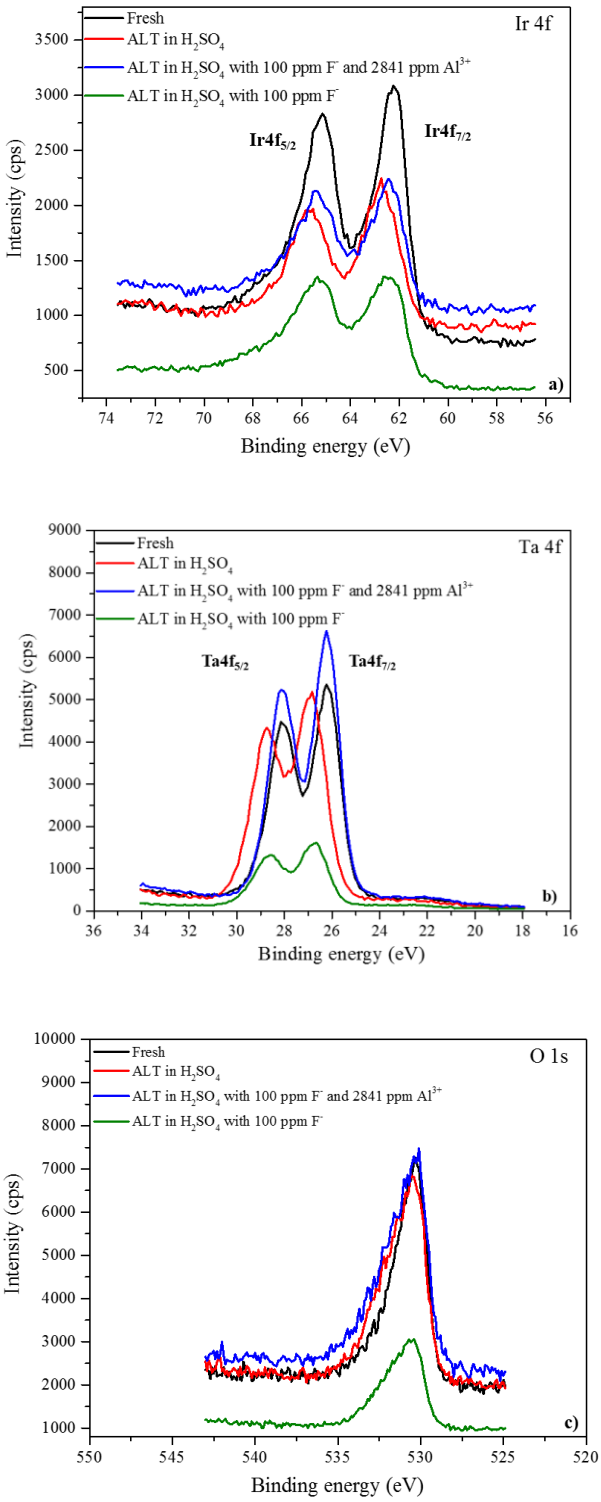

Figure 38. XPS spectrum of Ir (a), Ta (b), and O (c) for IrO_2-Ta_2O_5 coatings on as-received and galvanostatically stressed samples

Table 5. Binding energy for Ir 4f, Ta 4f and O 1s peaks in different samples.

Sample	**Binding energy (eV)**				
	Ir		Ta		O
	$4f_{5/2}$	$4f_{7/2}$	$4f_{5/2}$	$4f_{7/2}$	1s
Fresh	65.14	62.24	28.14	26.24	530.3
After ALT in H_2SO_4	65.54	62.74	28.74	26.94	530.6
After ALT in H_2SO_4 with 100 ppm fluoride	65.35	62.65	28.55	26.65	530.4
After ALT in H_2SO_4 with 100 ppm fluoride and 2841 ppm aluminum ions	65.24	62.44	28.14	26.24	530.1

Table 6. Intensity of Ir 4f, Ta 4f and O 1s peaks in different samples.

Sample	Intensity (cps)				
	Ir		Ta		O
	$4f_{5/2}$	$4f_{7/2}$	$4f_{5/2}$	$4f_{7/2}$	1s
Fresh	2831	3088	4475	5356	7255
After ALT in H_2SO_4	1970	2247	4336	5048	6895
After ALT in H_2SO_4 with 100 ppm fluoride	1351	1354	1325	1614	3052
After ALT in H_2SO_4 with 100 ppm fluoride and 2841 ppm aluminum ions	2075	2242	5235	6625	7475

The intensity of $4f_{5/2}$ and $4f_{7/2}$ peaks for Ir decreases when the as-received sample is subjected to ALT test in sulfuric acid solution, suggesting that Ir is removed from the solid. In the case of Ta, the intensity of these peaks decreases only slightly. For both elements, addition of fluoride to solution prior to ALT test results in a significant decrease in the intensity of both 4f

peaks suggesting the loss of oxide coating. Addition of aluminum ions to the fluoride containing sulfuric acid solution prior to ALT restores the Ir peak intensity to the value in plain sulfuric acid. The Ta peak intensity significantly increases under the same conditions and this is difficult to explain. Notwithstanding this strange result for Ta, it is reasonable to conclude that aluminum ions reduce the detrimental effects of HF through complexation.

The O 1s spectral region of the samples was asymmetric and hence was deconvoluted into four Gaussian-Lorentzian curves using the Kratos software (as presented in Figure 39). The four peak positions and the peak areas are tabulated in Table 7. The area under the curve with a peak at ~ 530.2 eV decreases in all samples subjected to ALTs. The relative areas under the four-curves are not significantly different for the treated samples.

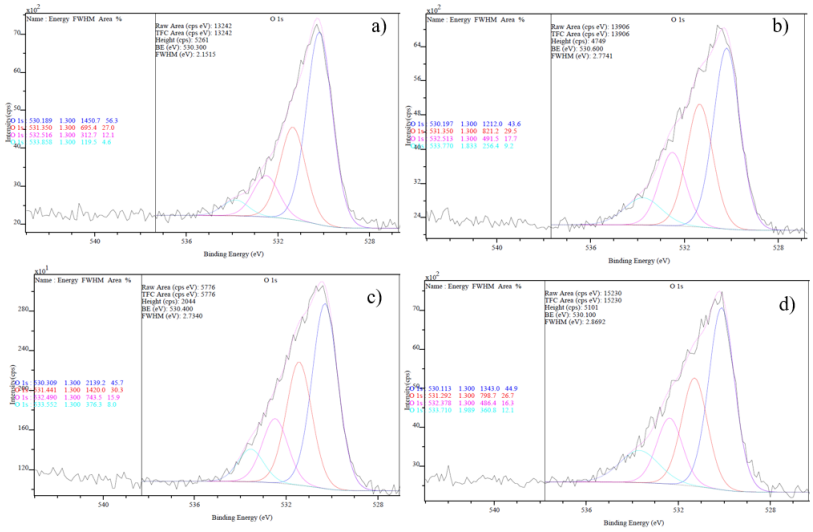

Figure 39. O 1s spectrum fitted with Gaussian-Lorentzian curves on the following samples: a) fresh, b) after an ALT in H_2SO_4, c) after an ALT in H_2SO_4 with 100 ppm fluoride, and d) after an ALT in H_2SO_4 with 100 ppm fluoride and 2841 ppm aluminum ions.

Table 7. O 1s peak positions, areas and % area on each sample.

Sample	O 1s		
	Peak position (eV)	Peak area (cps eV)	% area
Fresh	530.18	1450.7	56.3
	531.35	695.4	27
	532.52	312.7	12.1
	533.86	119.5	4.6
After ALT in H_2SO_4	530.19	1212	43.6
	531.35	821.2	29.5
	532.51	491.5	17.7
	533.77	256.4	9.2
After ALT in H_2SO_4 with 100 ppm fluoride	530.31	2139.2	45.7
	531.44	1420	30.3
	532.49	743.5	15.9
	533.55	376.3	8
After ALT in H_2SO_4 with 100 ppm fluoride and 2800 ppm aluminum ions	530.11	1343	44.9
	531.29	798.7	26.7
	532.38	486.4	16.3
	533.71	360.8	12.1

The % area listed in Table 7 indicates the percentage of the total area under the peak for each identified chemical state. Compared with the oxygen peak positions and areas reported in [37, 40] and the NIST database, the peak positions and areas listed in Table 7 correspond to the following species and peak positions: oxide, hydroxide, and water at 530 ± 0.5 eV, 531.5 ± 0.5 eV, and 533 ± 1 eV, respectively.

The peak at ~530.2 eV, which makes up the highest % of the O 1s area, can be ascribed to the oxygen in Ta_2O_5. This is somewhat surprising, considering that the EDS analysis indicated the oxide composition to be 70% iridium oxide. The O 1s peak at ~531.3 eV (contributing 26-30% of the area) fits the range for the Ir hydroxide species. Because the binding energies for O 1s in the OH groups present in $Ir(OH)_4$ and $IrO(OH)_2$ are 530.7 and 531.9 eV, respectively [37], the results indicate that the sample surface is hydroxylated. The remaining two peak positions most likely come from water. A surface composition analysis was also performed, and the results are listed in Table 8.

Table 8. Elemental analysis of the electrodes.

Element	**Mol%**			
	Fresh anode	Anode after ALT in H_2SO_4	Anode After ALT in H_2SO_4 with 100 ppm F	Anode After ALT in H_2SO_4 with 100 ppm F and 2841 ppm Al
IrO_2	42	28	57	24
Ta_2O_5	58	72	43	76

On the fresh anode, the IrO_2-to-Ta_2O_5 mol% is ~40:60, which is very different from the EDS analysis results. This difference in composition is caused by the shallow penetration depth (3-5 nm) that is typical in an XPS analysis; by contrast, the penetration depth is several microns in EDS characterization. For electrodes after ALTs in sulfuric acid alone and in sulfuric acid with added fluoride and aluminum, the IrO_2 component seems to preferentially dissolve over Ta_2O_5. On

the electrode after an ALT in the presence of 100 ppm fluoride, it is interesting to note that more Ta_2O_5 is lost than IrO_2 according to the near-surface analysis.

4.2.1.2 XRD analysis

X-ray diffraction was used to characterize the coatings before and after ALTs in the absence and presence of fluoride addition. The diffraction patterns for the fresh electrode sample and the galvanostatically stressed samples are presented in Figure 40 a-d.

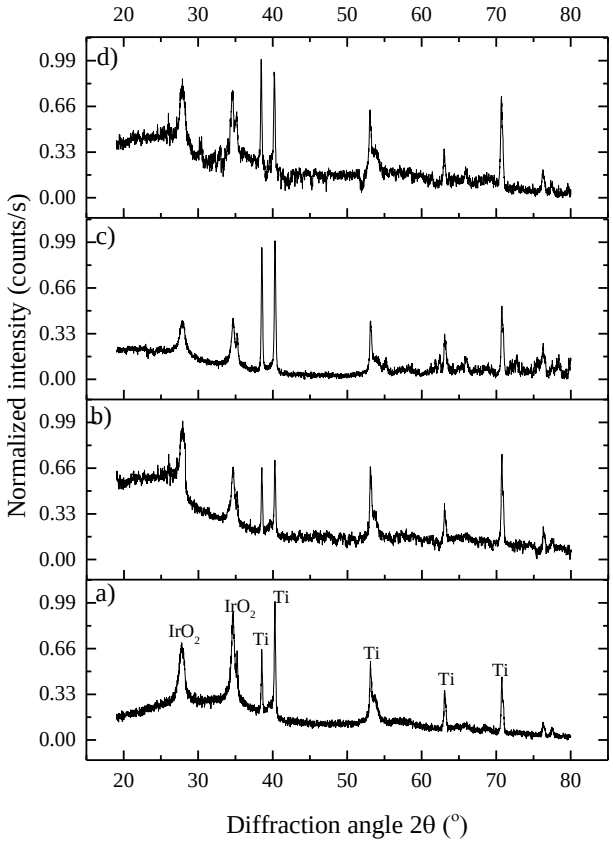

Figure 40. X-ray diffraction pattern for a fresh electrode (a), an electrode after an ALT in H_2SO_4 for 525 h (b), an electrode after an ALT in H_2SO_4 with 100 ppm fluoride addition for 207 h (c), and an electrode after an ALT in H_2SO_4 with 100 ppm fluoride and 2800 ppm aluminum ions for 538 h (d).

Compared with the fresh electrode, the diffraction patterns for the oxide coating on galvanostatically stressed electrodes have similar characteristic peaks for Ti and IrO_2. However, the peaks for IrO_2 have a relatively smaller intensity for the electrode after an ALT in the presence of 100 ppm fluoride, while the intensity of the Ti peaks is stronger, suggesting a loss in the amount of IrO_2 in the oxide coating.

4.2.2 Effect of iron addition to a fluoride-containing solution on electrode lifetime

In addition to aluminum ions, the presence of other metal cations such as iron has been reported in copper electrowinning baths [41]. Both of Fe^{3+} and Fe^{2+} have the ability to complex fluoride, however, as shown in the Appendix B, Fe^{3+} has higher stability constants of ferric fluoride complex species. Additionally, any Fe^{2+} would be oxidized to be Fe^{3+} near anode. Hence, only the effect of ferric ions addition on lifetime of electrode was investigated. As a first step in determining the role of Fe^{3+} on the accelerated lifetime, speciation and potential-pH diagrams were constructed. The thermodynamic data used for the construction of these diagrams are tabulated in the Appendix A.

Figure 41 displays the results of calculations for 2 M sulfate solutions in the pH range of -1 to 2 that contain 0.0105 M fluoride (200 ppm) and 0.0315 M Fe^{3+} (1760 ppm). The iron concentration was chosen based on the concentration of iron found in many electrowinning baths.

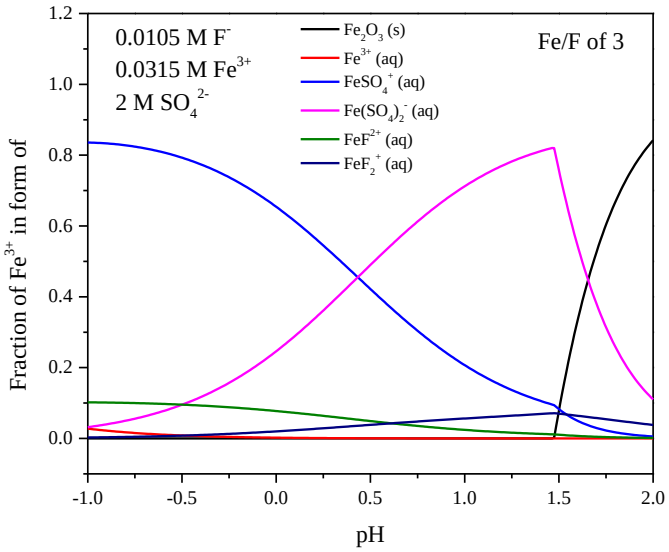

Figure 41. Predicted distribution of Fe^{3+} species in 2 M H_2SO_4 solution with 0.0105 M fluoride (200 ppm) and 0.0315 M Fe^{3+} (1760 ppm) ions.

Ferric ions form two types of sulfate complexes, cationic $FeSO_4^+$ and anionic $Fe(SO_4)_2^-$, and they are dominant in the pH range -1 to 0. Two cationic ferric fluoride complexes, FeF^{2+} and FeF_2^+, form in small amounts in the pH range -1.0 to 1.5. In a 2 M sulfuric acid solution at a pH of -0.54, approximately 10% of the added iron may be expected to be present in the FeF^{2+} form, with the remainder forming sulfate complexes. In other words, not all the added iron is available to complex fluoride.

The distribution of fluoride species in a 2 M sulfuric acid solution containing 0.0105 M fluoride (200 ppm) and 0.0315 M Fe^{3+} (1760 ppm) is depicted in Figure 42. Additionally, the fraction of fluoride in various forms at pH of -0.54 is given in Table 9.

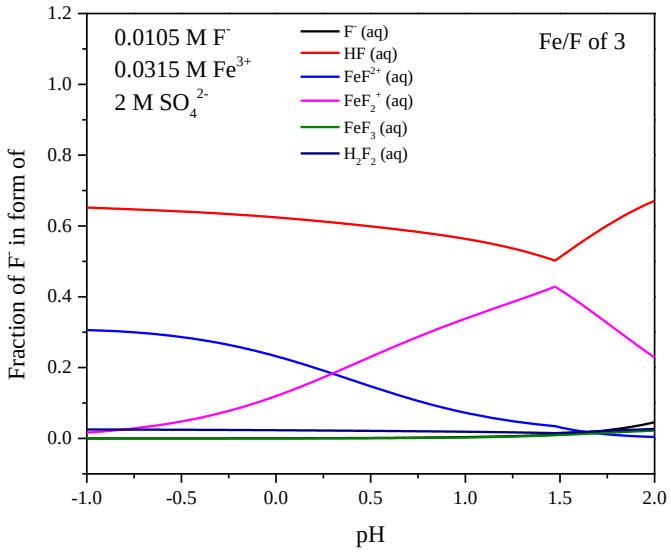

Figure 42. Predicted distribution of F^- species in a 2 M H_2SO_4 solution with 0.0105 M fluoride (200 ppm) and 0.0315 M Fe^{3+} (1760 ppm) ions.

Table 9. Distribution of added fluoride among various species in a 2 M sulfuric acid solution (pH of -0.54) upon ferric ion addition at an Fe-to-F molar ratio of 3.

pH	Fraction of F^- present in various forms					
	F^- (aq)	HF (aq)	FeF^{2+} (aq)	FeF_2^+ (aq)	FeF_3 (aq)	H_2F_2 (aq)
-0.54	0	0.642	0.289	0.044	0	0.025

In the distribution-pH diagram and Table 9, HF is evidently the dominant species among all fluoride species at a pH of -0.54, even with the addition of Fe^{3+} ions at an Fe-to-F molar ratio of 3. Aside from the HF species, most of the remaining free fluoride ions are complexed with Fe^{3+} to form FeF^{2+} and FeF_2^+. Very few fluoride ions are present as H_2F_2.

Because the ALTs were conducted at anodic potentials, a potential-pH diagram was constructed for the Fe-F-SO_4-water system to gain information on the effect of the anodic potential

on the stability regions of various species. This diagram, presented as Figure 43, shows that at a pH of -0.54, $FeSO_4^+$ is the most stable species at anodic potential values. (Note: Generally, these diagrams are drawn for potential values no higher than 2 V due to the breakdown of water to oxygen. In the diagram shown, potential values as high as 10 V were considered, and this may be questionable.)

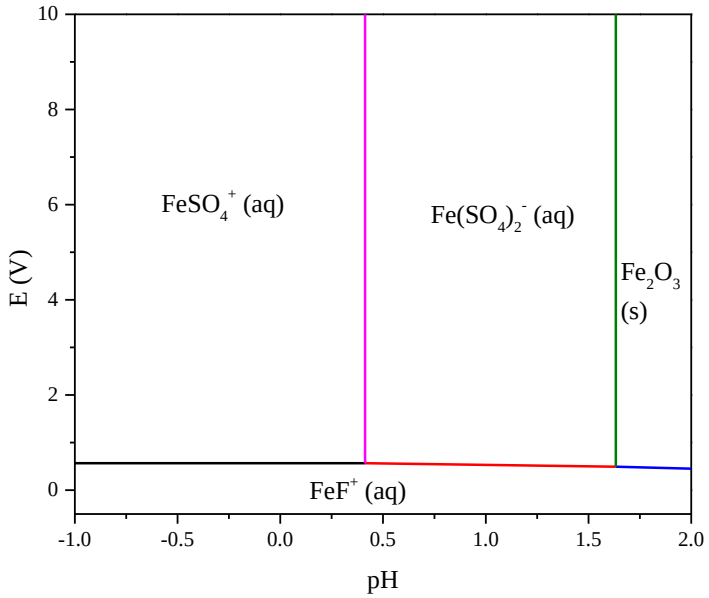

Figure 43. Pourbaix diagram for the Fe-F-SO_4-water system with 0.0105 M fluoride (200 ppm), 0.0315 M Fe^{3+} (1760 ppm), and 2 M SO_4^{2-} ions.

Because electrowinning baths typically contain aluminum and ferric ions as trace components, the effect of the simultaneous presence of these ions on speciation and free HF level was calculated. Typical Al^{3+} and Fe^{3+} levels in the baths are 400-2000 ppm (0.015-0.074 M) and 2000-3000 ppm (0.036-0.054 M), respectively. Calculations were performed to elucidate the effect of the ratio of the aluminum ion to ferric ion concentration on the free HF concentration with the

idea that adjusting this ratio may decrease free HF levels and hence improve anode life. The results of these calculations are shown in Table 10.

Table 10. Effect of the molar ratio of aluminum to iron on the free HF concentration in 2M sulfuric acid containing a total fluoride concentration of 100 ppm.

Molar ratio of Fe^{3+}:Al^{3+}:F^{-}	Predicted concentration (ppm)of HF at pH of -0.54
3:10:1	35
3:15:1	26.5
4:3:1	55.1
5:3:1	49.8
5:20:1	21.2

Addition of Fe^{3+} slightly increase the lifetime of electrodes in fluoride-containing solutions. However, the reaction of Fe^{3+} reduced to be Fe^{2+} will compete with Cu^{2+} reduction to Cu at cathode, which results in lower current efficiency in copper electrowinning. Hence, less Fe^{3+} is preferable; a molar ratio of Fe:Al:F at 3:15:1 was selected. The detailed speciation calculations are shown in Figure 44.

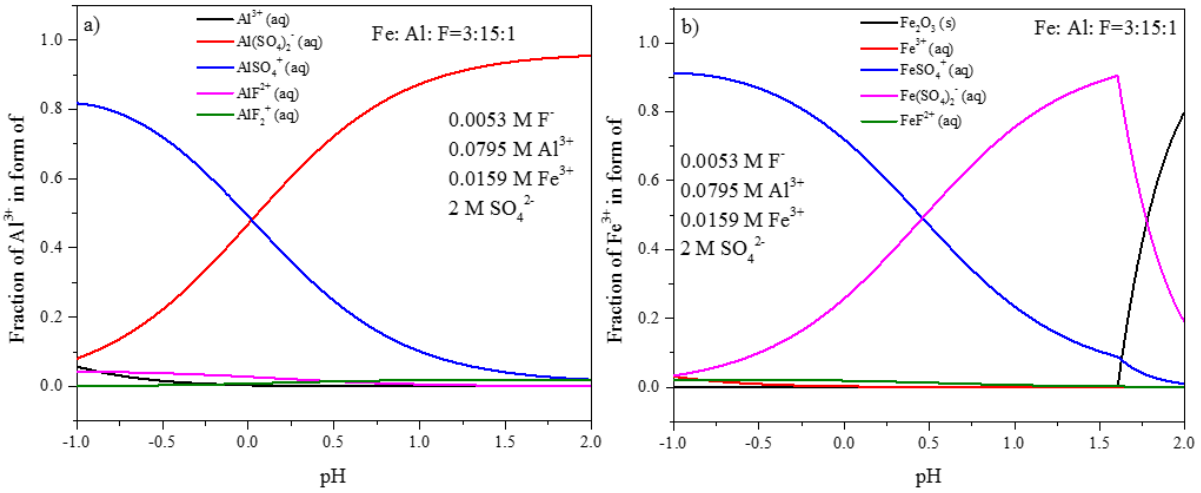

Figure 44. Distribution-pH diagrams of aluminum (a) and iron (b) species in a 2 M H_2SO_4 solution containing 100 ppm (0.0053 M) fluoride when 2144 ppm aluminum (0.0795 M) and 888 ppm iron (0.0159 M) ions are added at a molar ratio of Fe:Al:F of 3:15:1.

As depicted in Figure 44, both aluminum and ferric ions are preferentially complexed with sulfate and dominant in the pH range of -1 to 0. In addition, small amounts of aluminum and ferric fluoride complexes (AlF^{2+}, AlF_2^+, and FeF^{2+}) are present in the 2 M sulfuric acid solution at a pH of -0.54. The calculated fractional concentration of different fluoride species and the fraction of metal cations complexed with fluoride at a pH of -0.54 are listed in Tables 11 and 12.

Table 11. Predicted distribution of fluoride species at a pH of -0.54 upon aluminum and iron addition to a 2 M sulfate solution containing 100 ppm (0.0053 M) fluoride (molar ratio of Fe:Al:F of 3:15:1).

	Fraction of F^- present in various forms						
pH	HF(aq)	AlF^{2+} (aq)	AlF_2^+ (aq)	AlF_3 (aq)	FeF^{2+} (aq)	FeF_2^+ (aq)	AlF_4^- (aq)
-0.54	0.25	0.58	0.096	0.0003	0.065	0.002	0

Table 12. Fraction of metal cations complexed with sulfate and fluoride at a pH of -0.54 for a molar ratio of Fe:Al:F of 3:15:1.

	Fraction of cations	
	Fe^{3+}	Al^{3+}
Complexed with F^-	0.022	0.04
Complexed with SO_4^{2-}	0.97	0.94

Based on the calculated fractional concentration of different fluoride species and the fraction of metal cations complexed with fluoride, AlF^{2+} is the dominant metal cation fluoride complex. Compared with the fraction of iron complexed with fluoride, aluminum evidently has a greater ability to complex with fluoride. Hence, the addition of aluminum plays a key role in complexing more fluoride and compensating for the decreasing efficiency of copper deposition due to iron addition.

A Pourbaix diagram for fluoride-containing sulfate solution (F_T= 100 ppm) into which Al^{3+} and Fe^{3+} are added at a molar ratio of Fe: Al: F of 3:15:1 is shown in Figure 45. The dominant Al and Fe species at a pH of -0.54 are sulfate complexes. It may be recalled that speciation plots showed that less than 5% of these metal ions exist as fluoride; because of this, their stability regions do not show up in the diagram.

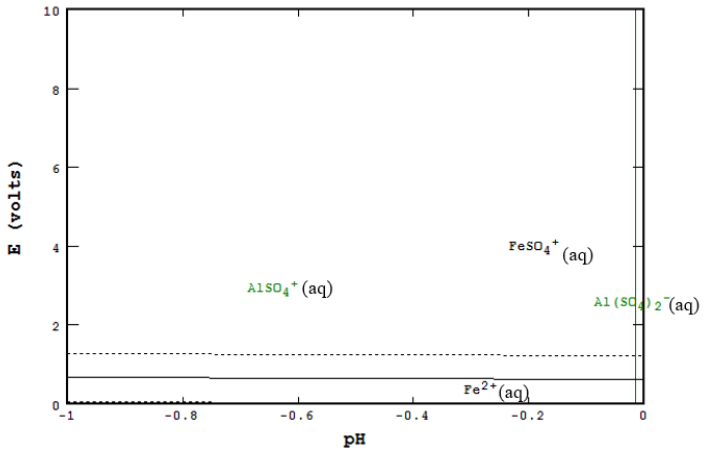

Figure 45. Pourbaix diagram for the Al-Fe-F-SO_4-water system when 2144 ppm aluminum (0.0795 M) and 888 ppm iron (0.0159 M) ions are added at a molar ratio of Fe:Al:F of 3:15:1 to a 2 M H_2SO_4 solution containing 100 ppm (0.0053 M) fluoride.

Multiple ALTs were performed on electrodes to determine the effect of Fe^{3+} and Al^{3+} ions on the lifetime in sulfuric acid solutions containing fluoride ions and to examine the usefulness of the speciation calculation predictions with respect to free HF level. The measured changes in the cell potential as a function of time are plotted in Figure 46, and the estimated accelerated lifetime for each electrode is listed in Table 13.

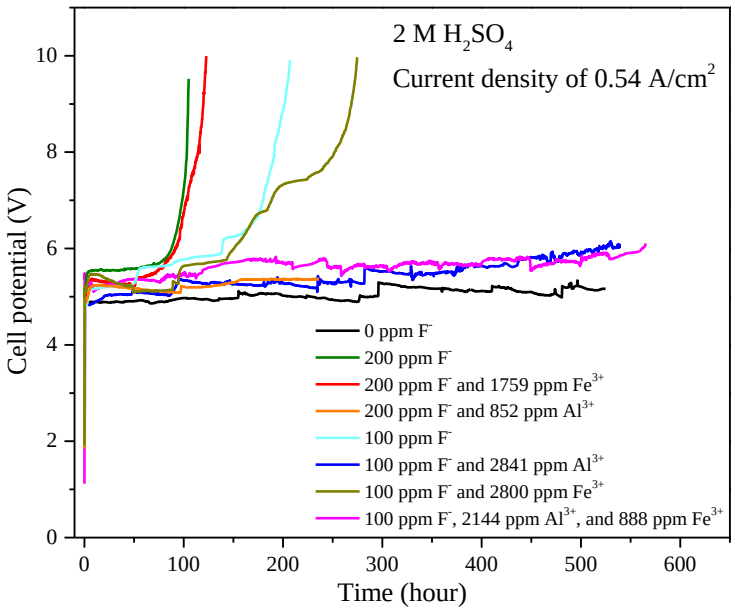

Figure 46. ALTs on electrodes in 2 M H_2SO_4 solutions with and without fluoride and metal cations.

Table 13. Summary of ALT results.

Concentration of fluoride	Concentration of metallic cation(s)	Molar ratio of cation(s) to fluoride	Test duration
0	0	0	525 h (No failure indicated)
100 ppm	0	0	207 h (Failure of anode)
100 ppm	2841 ppm Al^{3+}	Al^{3+}: F^- = 20:1	538 h (No failure indicated)
100 ppm	2800 ppm Fe^{3+}	Fe^{3+}: F^- = 9.4:1	275 h (Failure of anode)
100 ppm	2144 ppm Al^{3+} and 888 ppm Fe^{3+}	Fe: Al: F of 3:15:1	565 h (No failure indicated)
200 ppm	0	0	105 h (Failure of anode)
200 ppm	1759 ppm Fe^{3+}	Fe^{3+}: F^-=3:1	122 h (Failure of anode)
200 ppm	852 ppm Al^{3+}	Al^{3+}: F^-=3:1	236 h (No failure indicated)

In plain 2 M sulfuric acid solution, the electrodes showed no signs of failure for more than 500 h. In 100 ppm fluoride-containing sulfuric acid solutions, upon addition of approximately 2800 ppm aluminum ions, lifetime of electrode was extended to more than 500 hours. However, addition of 2800 ppm ferric ions to the same solution only increased the lifetime by approximately 70 hours. It is clear that at the level of 2800 ppm, aluminum ions are much more effective than ferric ions in extending the lifetime of the electrode. When both aluminum (~2100 ppm) and iron (~890 ppm) were added to the same solution, the lifetime of the electrode was more than 550 h, and no failure was observed.

In 200 ppm fluoride containing 2M sulfuric acid solution, the lifetime was decreased to 105 h. Aluminum ion addition, even at the level of 852 ppm, prolonged the lifetime of the electrode beyond 200 h. However, the addition of ferric ions at 1760 ppm (typical concentration found in electrowinning baths) failed to protect the electrode, and failure occurred at 122 h.

In summary, the addition of aluminum cations or a combination of aluminum and ferric ions can prolong the lifetime of electrodes in fluoride-containing solutions because complexation between the metal cations and fluoride ions reduces the presence of free HF, which is the primary cause of coating degradation.

4.3 Study on IrO_2-Ta_2O_5–coated Ti plate electrodes

One of the issues with IrO_2-Ta_2O_5 oxide coatings on a Ti mesh substrate is non-uniformity. To obtain more uniform IrO_2-Ta_2O_5 oxide coatings, Ti plate substrates were used.

4.3.1 Preparation method for IrO_2-Ta_2O_5–coated Ti plate electrodes

Two precursors, H_2IrCl_6 and $TaCl_5$, were dissolved in a butanol solution containing a resin and then applied to a Ti plate electrode using the brush-coating method. Four layers were applied and fired at 450°C to form mainly crystalline features. This process produces a 4-layer oxide-coated electrode. Another type of electrode was prepared using the same precursor mixture, but in this case, the Ti plate substrates were first brush-coated with 4 layers and fired at 450°C and then brush-coated with another 7 layers and fired at 400°C to form both crystalline and amorphous features (this is the same way the mesh electrodes are prepared). This process produces an 11-layer oxide-coated electrode.

4.3.2 XRD analysis of plate electrodes

XRD was used to characterize the crystalline structure of the IrO_2-Ta_2O_5 coating on the Ti plates. The diffraction patterns of a fresh 4-layer oxide-coated electrode and 11-layer oxide-coated electrode are shown in Figure 47.

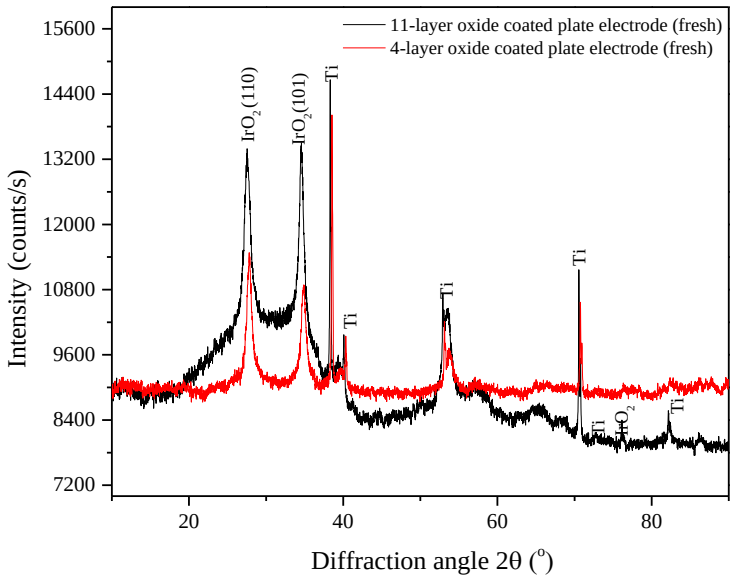

Figure 47. X-ray diffraction pattern of a fresh 4-layer oxide-coated electrode and 11-layer oxide-coated electrode.

The diffraction patterns produced by the coating on the plate electrodes are very similar to those formed on mesh electrodes. They contain reflections characteristic of two materials, Ti and IrO_2. No characteristic peaks for Ta_2O_5 were detected; this indicates the absence of crystallization of tantalum oxide during the thermal treatment of the coating. No significant differences were noted between the diffraction patterns of the oxide coatings on the 4-layer and 11-layer electrodes.

4.3.2 ALTs on plate electrodes

Various ALTs were carried out in 2 M sulfuric acid solutions in the absence and presence of fluoride at a constant current density of 0.54 A/cm^2. The measured cell potentials are plotted as a function of time in Figure 48. Table 14 lists the results of multiple ALTs.

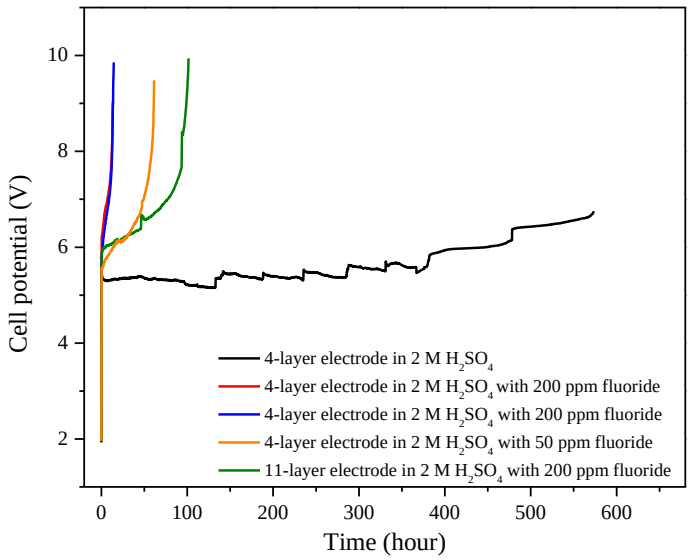

Figure 48. Results of ALTs conducted on plate electrodes in 2 M sulfuric acid solutions with and without fluoride.

Table 14. Summary of ALTs on plate electrodes.

Electrode	Concentration of fluoride	Test duration
4-layer oxide-coated Ti plate	0	573 h (No failure indicated)
4-layer oxide-coated Ti plate	200 ppm	13 h (Failure of anode)
4-layer oxide-coated Ti plate	200 ppm	14 h (Failure of anode)
4-layer oxide-coated Ti plate	50 ppm	61 h (Failure of anode)
11-layer oxide-coated Ti plate	200 ppm	101 h (Failure of anode)

Four-layer oxide-coated Ti plate electrodes did not fail after more than 550 h in a 2 M sulfuric acid solution. However, when 200 ppm fluoride was added to the sulfuric acid solution, the electrodes failed dramatically after only 13–14 h. When the fluoride level decreased to 50 ppm, the accelerated lifetime of the 4-layer oxide-coated Ti plate electrode was prolonged to approximately 60 h. For the 11-layer oxide-coated Ti plate electrode, the cell potential increased by 5 V at approximately 100 h, indicating failure of the electrode. The thickness of the coating indeed increases the lifetime. No significant differences were observed in the accelerated lifetime of the 11-layer oxide-coated Ti plate electrode and the mesh-based electrode.

4.4 Conclusions

The following conclusions can be drawn from the work described in this dissertation:

1. The lifetime of IrO_2-Ta_2O_5 coated electrodes was greatly reduced by the presence of fluoride in sulfuric acid solutions. The greater the amount of fluoride added, the shorter the anode lifetime. For example, the electrode did not fail for more than 500 hours in a plain 2

M sulfuric acid solution, whereas a failure occurred at ~100 hours in the presence of 200 ppm fluoride.

2. The overpotential for oxygen evolution of the coatings did not seem to be affected by stressing electrodes in fluoride-containing solutions. However, the current density for oxygen evolution on electrodes decreased after accelerated lifetime tests in fluoride-containing solutions.
3. The morphology of the virgin electrode consisted of dried-mud cracks, crystalline agglomerates, and flat areas. After ALT in a fluoride-containing solution, pores and deep cracks formed. Complete removal and localized thinning of the oxide coating were seen in some locations. EDS analysis indicated that the molar ratio of IrO_2 to Ta_2O_5 in the coating did not change during thinning of the coating.
4. XPS analysis of the coatings subjected to ALT in fluoride containing sulfuric acid indicated that the intensity of the Ir 4f, Ta 4f, and O 1s peaks decreased, suggesting thinning of the coating. The analysis O 1s spectrum showed that most of the oxygen is bound to Ta as Ta_2O_5 in the surface layer (~ 2-3 nm). This is somewhat surprising given that there is more iridium than tantalum in the bulk of the coating.
5. Based on speciation calculations, the majority (95-99%) of the fluoride species should be present as HF when fluoride is added to sulfuric acid solutions. Pourbaix diagrams constructed for the Ir-F-water and Ta-F-water system show that at high anodic potentials, the most stable form of Ir is IrF_6 (s) while the most stable form of Ta is TaO_2^+. Hence the coating degradation may be postulated to occur by HF attack of IrO_2 to form solid IrF_6 and Ta_2O_5 reaction with H^+ from sulfuric acid to form aqueous TaO_2^+. Even though IrF_6 is a solid, it did not seem to protect the substrate probably due to erosion caused by oxygen

bubbles generated at anode. The rise in cell potential during end of (accelerated) life of coating is due to passivation of Ti substrate exposed to solutions.

6. A strategy was developed to prolong the lifetime of electrodes in fluoride-containing solutions: reduce the amount of HF present by adding metal cations such as Al^{3+} and Fe^{3+} to complex free fluoride ions in solution. When Al^{3+} or Fe^{3+} ions were added to 200 ppm fluoride-containing solutions at a molar ratio of cation to F of 3, the ferric ions did not have much effect on extension of lifetime, whereas the aluminum ions prolonged the lifetime beyond 200 hours. As in 100 ppm fluoride-containing solutions, when a similar amount (2800 ppm) of metal cation was added, anode lifetime was extended for more than 500 hours with aluminum addition, while the electrode failed at 275 hours in the presence of added ferric ions. When a combination of metal cations with a molar ratio of Fe:Al:F of 3:15:1 was added, the lifetime of the electrode was successfully prolonged to beyond 500 hours in a 100 ppm fluoride-containing solution. Hence, either aluminum ions alone or a combination of aluminum and ferric ions could be used to extend the electrode lifetime.
7. Additional investigations on IrO_2-Ta_2O_5 coated Ti plate substrates were conducted. Results indicate that in the 200ppm fluoride-containing solutions, the 4-layer oxide-coated electrode failed dramatically after only 13-14 hours, whereas the 11-layer oxide-coated electrode failed at approximately 100 hours. A thicker coating increased the lifetime, as expected. However, no significant differences were observed in the accelerated lifetime of the 11-layer oxide-coated Ti plate electrode and the mesh-based electrode.

4.5 Future work

In the current work, the effects of fluoride and metal cation addition on the electrochemical behavior of IrO_2-Ta_2O_5 coatings on Ti mesh electrodes have been investigated. The current density

used was 0.54 A/cm^2, which is actually three times larger than the current density used in industry. Changing the current density used in ALTs may cause the lifetime of the electrode to vary. Therefore, a study of the effect of the current density used in ALTs on electrode lifetime is worth considering.

In addition to the trace-level metal cations reportedly present in copper electrowinning baths, chemical additives used to improve specific aspects of the process performance are present in low concentrations. Examples include acid mist suppressors and grain refinement additives. The mist suppressor is a fluorocarbon surfactant that is added in concentrations of 20-30 ppm and is used to prevent 'bursting' of oxygen bubbles formed during the electrowinning process. The grain refinement additive is a type of modified corn starch (hydroxypropyl starch ether) present in concentrations of ~30 ppm in electrowinning baths that is used to enhance the quality of the deposited copper. Because the grain refinement additive is a hydrophilic compound, it can adsorb on the anode surface and possibly bind with multivalent cations. Very few studies have been reported on the effects of acid mist suppressors and/or grain refinement additive on the electrode lifetime and oxygen evolution reaction. Hence, an investigation of the influence of additives on the electrochemical and microstructural properties of IrO_2-Ta_2O_5 coatings on Ti mesh electrodes would be a valuable extension of the current work.

APPENDIX A: Thermodynamic data used to conduct speciation calculations from STABCAL

In this project, Pourbaix diagrams and distribution-pH diagrams were constructed using the computer software STABCAL. The species and their Gibbs formation values from three databases—Minteq, Critical, and NBS from the software are listed in Table 15.

Table 15. Thermodynamic data used to conduct speciation calculations from STABCAL.

Species	Standard free energy of formation ΔG^0 (kJ/mol)	Species	Standard free energy of formation ΔG^0 (kJ/mol)
$Fe(OH)_2^+$ (aq)	-438.00	$Al(OH)_2^+$ (aq)	-899.03
$Fe(OH)_3$ (aq)	-659.30	$Al(OH)_3$ (aq)	-1106.15
$Fe(OH)_3$ (s)	-699.18	$Al(OH)_3$ (s) alpha	-1149.09
$Fe(OH)_3$ (s) aged	-700.16	$Al(OH)_3$ (s) am	-1134.74
$Fe(OH)_3$ (s) Ferrihydrite	-697.82	$Al(OH)_3$ (s) Gibbsite	-1152.21
$Fe(OH)_3$ (s) Ferrihydrite-aged	-700.73	$Al(OH)_3$ (s) Soil	-1149.06
$Fe(OH)_3$ (s) ppt	-696.49	$Al(OH)_4^-$ (aq)	-1305.29
$Fe(OH)_4^-$ (aq)	-842.45	$Al(SO_4)_2^-$ (aq)	-2005.45
$Fe(SO_4)_2^-$ (aq)	-1524.49	$Al_{13}O_4(OH)_{24}^{7+}$ (aq)	-12378.44
$Fe_2(OH)_2^{4+}$ (aq)	-467.27	$Al_2(OH)_2^{4+}$ (aq)	-1400.34
$Fe_2(SO_4)_3$ (s)	-2263.62	$Al_2(SO_4)_3$ (s)	-3099.94
Fe_2O_3 (s) (Hematite)	-742.19	$Al_2(SO_4)_3 \cdot 6H_2O$ (s)	-4622.06
Fe_2O_3 (s) (Magnemite)	-684.33	Al_2O_3 (s)	-1569.21
$Fe_3(OH)_4^{5+}$ (aq)	-926.72	Al_2O_3 (s) Corundum	-1582.30
Fe^{3+} (aq)	-4.69	Al_2O_3: $3H_2O$ (s) Gibbsite	-2310.21
$FeOH^{2+}$ (aq)	-229.41	Al_2O_3: H_2O (s) Boehmite	-1831.70
FeOOH (s) alpha	-476.89	Al_2O_3: H_2O (s) Diaspore	-1841.78
FeOOH (s) Lepidocrocite	-471.13	$Al_3(OH)_4^{5+}$ (aq)	-2324.24
$FeSO_4^+$ (aq)	-772.70	Al^{3+} (aq)	-485.00
$H_2Fe_3(SO_4)_2(OH)_7$ (s) Jarosite-H	-3193.36	$Al_4(OH)_{10}SO_4$ (s)	-4926.02
$HFeO_2$ (s) Goethite	-476.15	$AlOH^{2+}$ (aq)	-694.10
AlF^{2+} (aq)	-803.00	$AlOHSO_4$ (s)	-1484.87

AlF_2^+ (aq)	-1112.99	AlOOH (s) Boehmite	-910.29
AlF_3 (aq)	-1414.00	$AlSO_4^+$ (aq)	-1251.22
AlF_3 (s)	-1424.99	$HAlO_2$ (s) Diaspore	-920.03
AlF_4^- (aq)	-1710.89	IrO_2 (s)[a]	-161.13
$AlOHF_2$ (s)	-1277.38	SO_4^{2-} (aq)	-744.53
F^- (aq)	-278.78	HSO_4^- (aq)	-755.91
FeF^{2+} (aq)	-322.59	IrF_6 (s)	-461.56
FeF_2^+ (aq)	-628.39	Ta_2O_5 (s)	-1911.20
FeF_3 (aq)	-919.26	TaO_2^+ (aq)	-842.59
H_2F_2 (aq)	-596.23	TaF_5 (aq)	-1131.70
HF (aq)	-296.82	TaF_6^- (aq)	-1431.70
HF_2^- (aq)	-578.08	TaF_7^{2-}(aq)	-1729.49

Note:

a. Calculated from reference [42].

APPENDIX B: Stability constants of fluoride and sulfate complexes with Al^{3+} and Fe^{3+}

Stability constant of fluoride and sulfate complexes found in literature are listed in Table 16.

Table 16. Stability constant of fluoride and sulfate complexes at 25 °C [43].

Ions	Species	Log K
F^-	HF (aq)	3.3
	HF_2^- (aq)	0.84
Al^{3+}	AlF^{2+} (aq)	6.69
	AlF_2^+ (aq)	5.35
	AlF_3 (aq)	3.68
	AlF_4^- (aq)	2.75
	$AlSO_4^+$ (aq)	3.01
	$Al(SO_4)_2^-$ (aq)	1.89
Fe^{3+}	FeF^{2+} (aq)	5.19
	FeF_2^+ (aq)	9.12
	FeF_3 (aq)	12.05
	$FeSO_4^+$ (aq)	2.23
	$Fe(SO_4)_2^-$ (aq)	3.26
Fe^{2+}	FeF^+ (aq)	3.1
	FeF_2 (s)	4.6
	$FeSO_4$ (aq)	2.72
Cu^{2+}	CuF^+ (aq)	0.84

APPENDIX C: Procedure for conducting accelerated life test using PAR 2273

Sample preparation

1) Below is the figure of IrO_2-Ta_2O_5 coated Ti mesh electrode. First, use a plier to create a hole on the electrode for setting up electrical contacts. Then insert 304 stainless steel made terminal rings, nuts and bolts on the electrode and Ti expanded mesh (cathode). Apply the anti-oxidation grease and wrap with anti-corrosive tape (5491 PTFE, 3M).
2) Rinse with IPA and DI water on exposed areas of anode and cathode.

Figure 1

3) Prepare a solution of 2 M H_2SO_4 containing a certain level of fluoride in test beaker and recirculate the solution. Start experiment until the temperature of the solution is at ambient temperature.

Accelerated life test

Accelerated life test uses the galvanostatic method, which is applying a constant current density on anode and monitoring the changes in cell potential between anode and cathode.

4) Use a two electrode system by setting IrO_2-Ta_2O_5 coated Ti mesh electrode as working electrode and shorting counter and reference electrodes using a Ti mesh. The electrochemical cell setup is shown in Figure 2. Use alligator clips to connect anode and cathode to PAR 2273.
5) Turn on PAR 2273, press **Cell enable,** and turn on current booster. Details on the connection of electrode are shown in Figure 3.

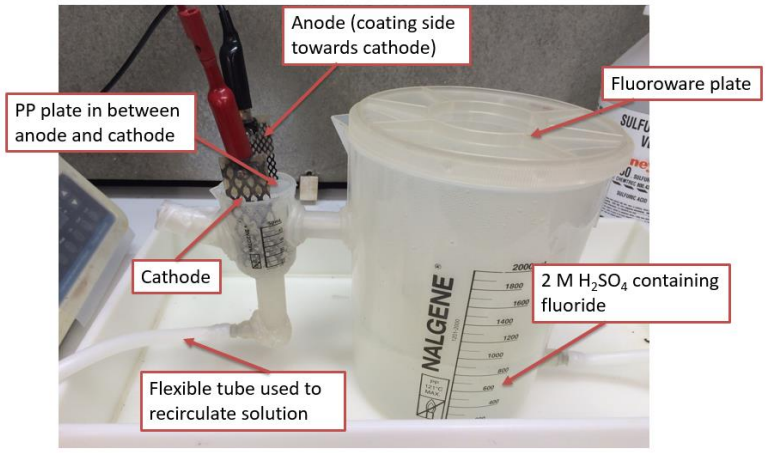

Figure 2.

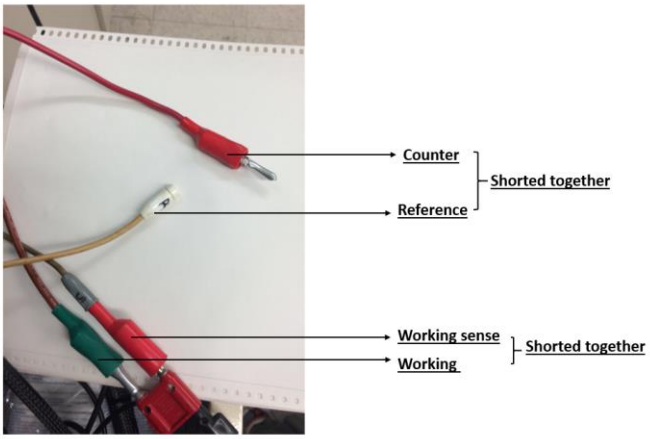

Figure 3.

6) Start galvanostatic measurement.
    a. Open **PowerSuite** on the desktop. Click Experiment→New.

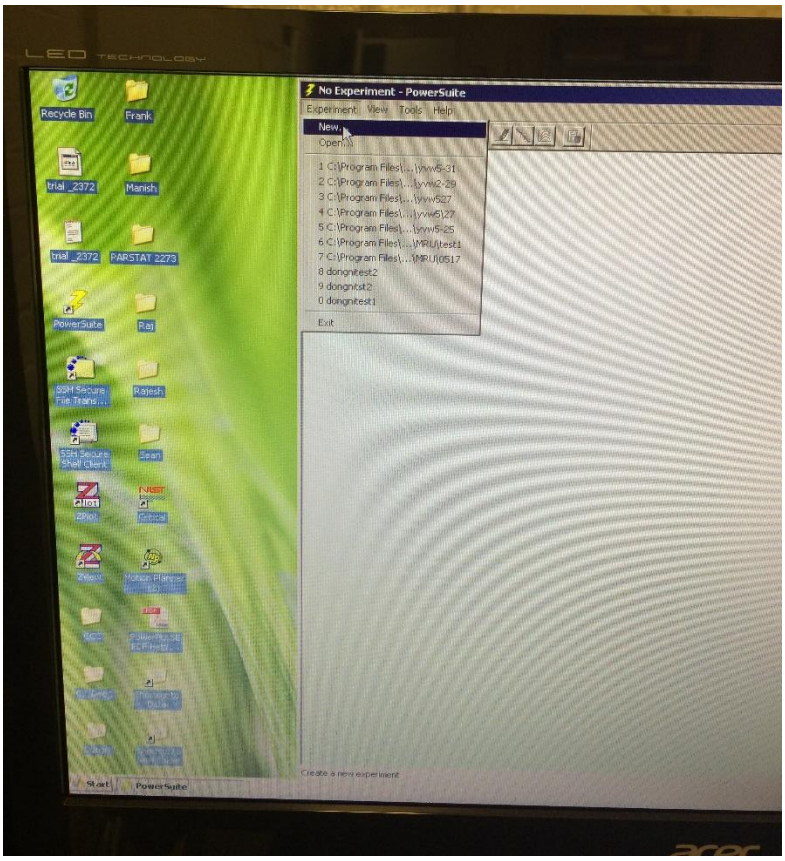

b. Expand **PowerCorr→** Click **Galvanostatic** and name your experiment. Then click Next.

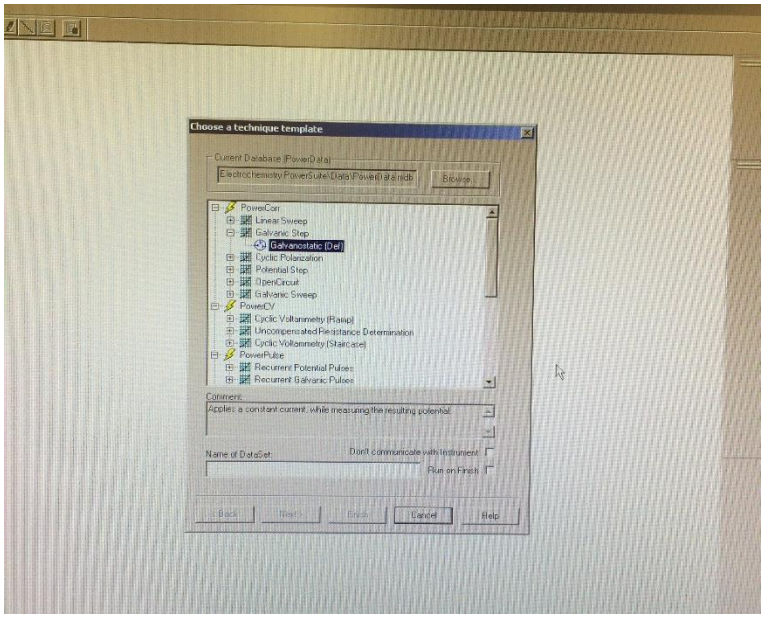

c. Check **PowerBooster**, Reference electrode click type of user for accelerated life test. Then click Next.

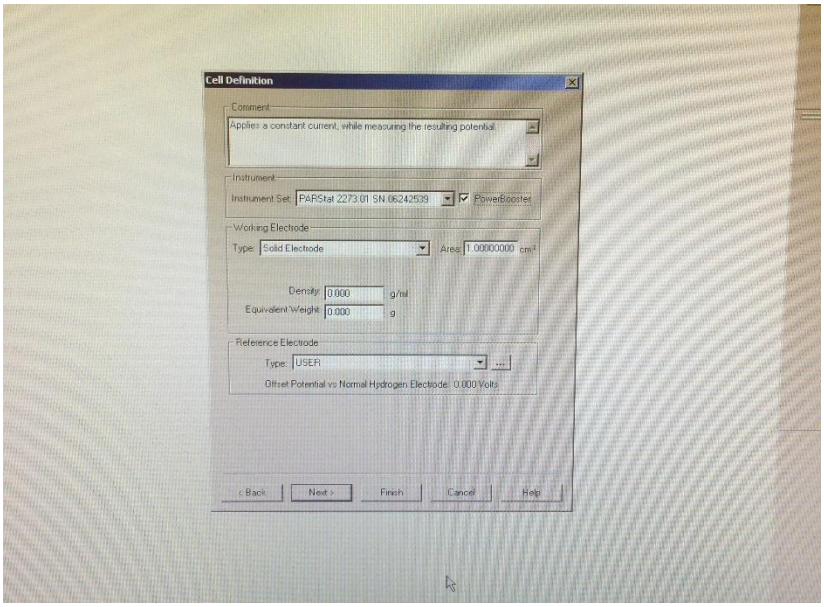

d. Input current you use for current step (current density times immersion area of anode). Step time is the duration of experiment, Time per Point is how long you would like to have one data point. Decide the frequency of data point to set the time per point. **Please note that the maximum data points PowerSuite can collect is 1000. Normally I set the Step time as 100 hours, then I stopped the experiment to move tube. Then I reset experiment again for 100 hours.** Then click on Next.

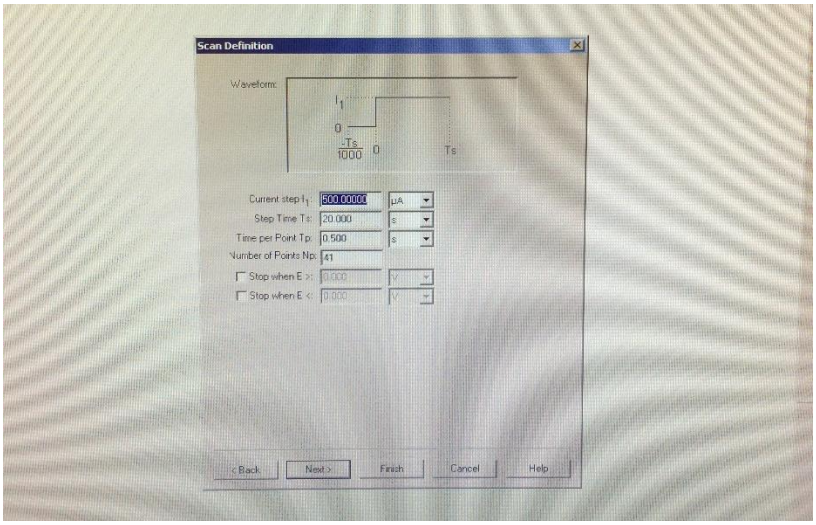

e. In this window, it indicates that PAR will measure OCP as required. Then click on Next.

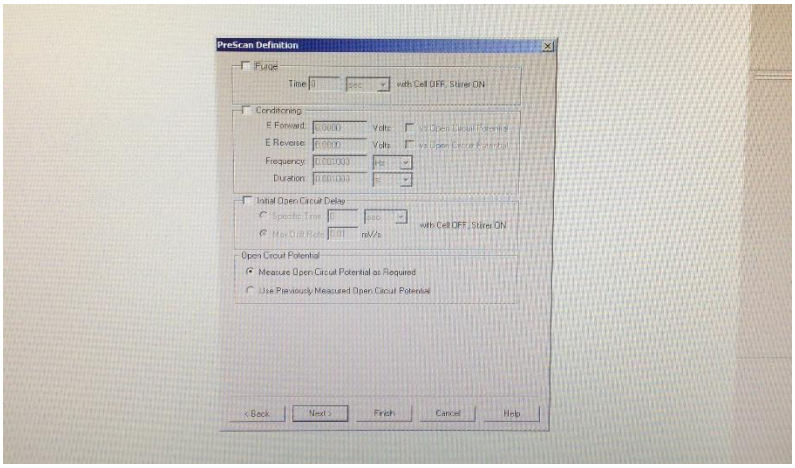

f. Check **Custom Pstat Control** and **Override Auto E Feedback** to ensure resetting Pstat before starting, turning off cell when done, and maximizing stability. Click Finish.

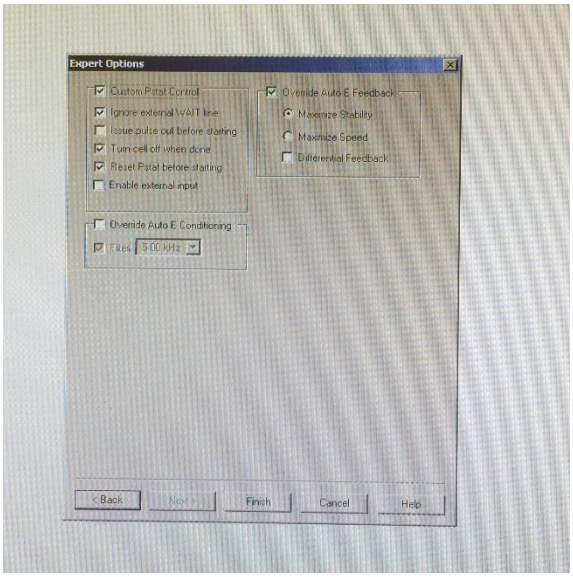

g. Wait until PAR is booting and when the icon ►shows, it means you can start experiment now. Click ►, a plot of E vs. time will present gradually based on the Time per Point you set before.

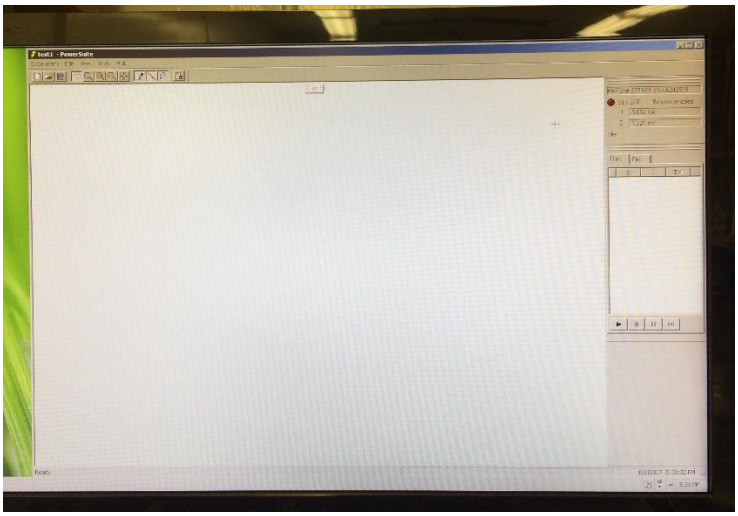

7) Once experiment is over, press the **Cell Enable** to disable it and turn off PAR 2273. Then turn off the current booster. Experiment data will be saved as a txt file, import it to excel and get your plot.
8) Stop recirculating solution, dump the solution to the acid waste bucket, clean electrodes and workplace.

REFERENCES

1. https://www.fcx.com/resources/fmi/index.html
2. Z. S. Msindo, V. Sibanda, J. H. Potgieter, “Electrochemical and physical characterization of lead-based anodes in comparison to Ti– (70%) IrO_2/ (30%) Ta_2O_5 dimensionally stable anodes for use in copper electrowinning,” *J. Appl. Electrochem.*, **40**, 691-699 (2010).
3. J. A. V. Butler, "Studies in heterogeneous equilibria. II. The kinetic interpretation of the Nernst theory of electromotive force," *Trans. Faraday Soc*. (advance proof), (1924).
4. J. A. V. Butler, "Studies in heterogeneous equilibria. III. A kinetic theory of reversible oxidation potential at inert electrodes," *Trans. Faraday Soc*. (advance proof), (1924).
5. T. Erdey-Gruz and M. Volmer, “The theory of hydrogen overvoltage,” *Z. Physik. Chem*., **150**(Abt. A), 203-213 (1930).
6. C. M. A. Brett and A. M. O. Brett, Electrochemistry: principles, methods, and applications, Oxford science publications., Oxford University Press, Oxford; New York, xxviii, 427, (1993).
7. W. Huang, “Fundamental studies on the removal of copper in hydroxylamine based chemistries of interest to copper chemical-mechanical planarization”, Ph.D. dissertation, The University of Arizona, Tucson, AZ (2003).
8. M. G. Fontana, *Corrosion Engineering,* 3rd ed, McGraw-Hill, New York, (1986).
9. H. Yang, Z. Zeng, Y. Hu, and L. Chen, “Electrochemical behavior of Ir-Ta oxide coating electrode in sulfate electrolyte,” *Nonferrous Metals (Extractive Metallurgy)*., **05**, 40-43 (2009).

10. J. Krýsa, L. Kule, R. Mráz, I. Roušar, "Effect of coating thickness and surface treatment of titanium on the properties of IrO_2–Ta_2O_5 anodes," *J. Appl. Electrochem.,* **26**, 999-1005 (1996).
11. CH. Comninellis, G. P. Vercesi, "Characterization of DSA®-type oxygen evolving electrodes: choice of a coating," *J. Appl. Electrochem.,* **21**, 335-345 (1991).
12. M. Morimitsu, H. Tamura, M. Matsunaga, R. Otogawa, "Polarization behaviour and lifetime of IrO_2–Ta_2O_5–SnO_2/Ti anodes in p-phenolsulfonic acid solutions for tin plating," *J. Appl. Electrochem.,* **30**, 511-514 (2000).
13. C. H. Yang, C. C. Lee, T. C. Wen, "Hypochlorite generation on Ru–Pt binary oxide for treatment of dye wastewater," *J. Appl. Electrochem.,* **30**, 1043-1051 (2000).
14. M. Rubel, R. Haasch, P. Mrozek, *et al*, "Characterization of IrO_2-SnO_2 thin layers by electron and ion spectroscopies," *Vacuum.,* **45**, 423-427 (1994).
15. S. Trasatti, G. Lodi, in S. Trasatti (Eds.), *Electrodes of Conductive Metallic Oxides Part A*, Amsterdam: Elsevier (1980).
16. J. M. Hu, H. M. Meng, J. Q. Zhang, C. N. Cao, "Degradation mechanism of long service life Ti/IrO_2-Ta_2O_5 oxide anodes in sulphuric acid," *Corros Sci*., **44**, 1655-1668 (2002).
17. A. De Oliveira-Sousa, M. A. S. Da Silva, S. A. S. MacHado, L. A. Avaca, P. De Lima-Neto, "Influence of the preparation method on the morphological and electrochemical properties of Ti/IrO_2-coated electrodes," *Electrochim. Acta.,* **45**, 4467-4473 (2000).
18. L. Xu, Y. Xin, J. Wang, "A comparative study on IrO_2-Ta_2O_5 coated titanium electrodes prepared with different methods," *Electrochim. Acta*., **54**, 1820-1825 (2009).
19. L.K. Xu, J. D. Scantlebury, "Electrochemical surface characterization of IrO_2-Ta_2O_5 coated titanium electrodes in Na_2SO_4 solution," *J. Electrochem. Soc*., **150**, B288-B293 (2003).

20. L.K. Xu, J. D. Scantlebury, "A study on the deactivation of an IrO_2-Ta_2O_5 coated titanium anode," *Corros. Sci*., **45**, 2729-2740 (2003).
21. B. S. Li, A. Lin, F. X. Gan, "Preparation and electrocatalytic properties of Ti/IrO_2-Ta_2O_5 anodes for oxygen evolution," *Trans. Nonferrous Met. Soc. China*., **16**, 1193-1199 (2006).
22. R. F. Savinell, R. L. Zeller III, and J. A. Adams, "Electrochemically active surface area. Voltammetric charge correlations for ruthenium and iridium dioxide electrodes," *J. Electrochem. Soc*., **137**, 489-494 (1990).
23. L. K. Xu and J. D. Scantlebury, "Microstructure and electrochemical properties of IrO_2-Ta_2O_5-coated titanium anodes," *J. Electrochem. Soc*., **150**, B254-B261 (2003).
24. M. Morimitsu, C. Murakami, K. Kawaguchi, R. Otogawa, M. Matsunaga, "Stability of iridium oxide-tantalum oxide coated titanium electrodes for oxygen evolution in alkaline solutions," *J. New Mater. Electrochem. Syst*., **7**, 323-327 (2004).
25. E. Mahe, D. Devilliers, "Surface modification of titanium substrates for the preparation of noble metal coated anodes," *Electrochim. Acta*., **46**, 629-636 (2000).
26. A. J. Terezo, E. C. Pereira, "Preparation and characterisation of Ti/RuO2 anodes obtained by sol-gel and conventional routes," *Mater. Lett*., **53**, 339-345 (2002).
27. M. Morimitsu, T. Yamaguchi, N. Oshiumi, T. Zhang, "Energy-efficient electrowinning process with smart anode comprising nano-oxide catalyst," *Proceedings of EMC.*, 975-984 (2011).
28. Y. Matsumoto and E. Sato, "Electrocatalytic properties of transition metal oxides for oxygen evolution reaction," *Mater. Chem. Phys*., **14**, 397-426 (1986).

29. J. M. Hu. J. Q. Zhang, and C. N. Cao, "Oxygen evolution reaction on IrO_2-based DSA® type electrodes: kinetics analysis of Tafel lines and EIS," *Int. J. Hydrogen Energy*., **29**, 791-797 (2004).

30. G. N. Martelli, R. Ornelas, and G. Faita, "Deactivation mechanism of oxygen evolving anodes at high current density," *Electrochim. Acta*., **39**, 1551-1558 (1994).

31. L. M. Da Silva, D. V. Franco, L. A. De Faria, and J. F. C. Boodts, "Surface, kinetics and electrocatalytic properties of Ti/ (IrO_2 + Ta_2O_5) electrodes, prepared using controlled cooling rate, for ozone production," *Electrochim. Acta*., **49**, 3977-3988 (2004).

32. L. A. Da Silva, V. A. Alves, M. A. P. Da Silva, S. Trasatti, J. F.C. Boodts, "Morphological, chemical, and electrochemical properties of Ti/ (TiO_2 + IrO_2) electrodes," *Can. J. Chem*., **75**, 1483-1493 (1997).

33. Z. Yan, Y. Zhao, Z. Zhang, *et al*, "A study on the performance of IrO_2–Ta_2O_5 coated anodes with surface treated Ti substrates," *Electrochim. Acta*., **157,** 345-350 (2015).

34. F. Ye, J. Li, X. Wang, and *et al*, "Electrocatalytic properties of Ti/Pt-IrO_2 anode for oxygen evolution in PEM water electrolysis," *Int. J. Hydrogen Energy*., **35**, 8049-8055 (2010).

35. Y. Xin, L. Xu, and J. Wang, "Effect of sintering temperature on microstructure and electrocatalytic properties of Ti/IrO_2–Ta_2O_5 anodes by pechini method," *Rare Metal Mat Eng*., **39**, 1903-1907 (2010).

36. Z. Ren, S. Quan, J. Gao, and *et al*, "The electrocatalytic activity of IrO_2–Ta_2O_5 anode materials and electrolyzed oxidizing water preparation and sterilization effect," *RSC Adv*., **5**, 8778-8786 (2015).

37. S. Ardizzone, C. L. Bianchi, G. Cappelletti, M. Ionita, and *et al*, "Composite ternary SnO_2-IrO_2-Ta_2O_5 oxide electrocatalysts," *J. Electroanal. Chem.*, **589**, 160-166 (2006).

38. J. M. Hu, J. X. Wu, H. M. Meng, Y. R. Zhu, D. B. Sun, and D. J. Yang, "Investigation of surface morphology, structure and electrocatalytic properties for O_2 evolution of titanium based IrO_2+Ta_2O_5 coatings," *Acta Metall. Sin.*, **13**, 849-856 (2000).
39. Anatoly Agulyansky, *Chemistry of tantalum and niobium fluoride compounds.*, Boston, Elsevier, 257 (2004).
40. R. Sanjinés, A. Aruchamy, and F. Lévy, "Thermal stability of sputtered iridium oxide films," *J. Electrochem. Soc.*, **136**, 1740-1743 (1989).
41. L. Sicupira, T. Veloso, F. Reis, and V. Leão, "Assessing metal recovery from low-grade copper ores containing fluoride," *Hydrometallurgy.*, **109**, 202-210 (2011).
42. C. B. Lee, B. S. Kang, A. Benayad, and *et al*, "Effects of metal electrodes on the resistive memory switching property of NiO thin films," *Appl. Phys. Lett.*, **93**, 042115 (2008).
43. Högfeldt, Erik. *Stability constants of metal-ion complexes: Part A: Inorganic ligands.*, New York, Pergamon Press, 1982.